BJP British Journal of Pharmacology

DOI:10.1111/bph.12992
www.brjpharmacol.org

RESEARCH PAPER

Synthesis and SAR studies of novel 6,7,8-substituted 4-substituted benzyloxyquinolin-2(1*H*)-one derivatives for anticancer activity

Yi-Fong Chen[1,2], Yi-Chien Lin[2], Susan L Morris-Natschke[3], Chen-Fang Wei[2], Ting-Chen Shen[2], Hui-Yi Lin[2], Mei-Hua Hsu[2], Li-Chen Chou[2], Yu Zhao[3], Sheng-Chu Kuo[1,2], Kuo-Hsiung Lee[3,4]* and Li-Jiau Huang[1,2]*

[1]*The Ph.D. Program for Cancer Biology and Drug Discovery, China Medical University and Academia Sinica, Taichung, Taiwan,* [2]*School of Pharmacy, China Medical University, Taichung, Taiwan,* [3]*Natural Products Research Laboratories, UNC Eshelman School of Pharmacy, University of North Carolina, Chapel Hill, NC, USA, and* [4]*Chinese Medicine Research and Development Center, China Medical University and Hospital, Taichung, Taiwan*

Correspondence
Li-Jiau Huang, School of Pharmacy, China Medical University, No.91 Hsueh-Shih Road, Taichung, 40402, Taiwan. E-mail: ljhuang@mail.cmu.edu.tw or Kuo-Hsiung Lee, Natural Products Research Laboratories, UNC Eshelman School of Pharmacy, University of North Carolina, Chapel Hill, NC 27599-7568, USA. E-mail: khlee@unc.edu

*Both authors contributed equally to this work.

Received
9 June 2014
Revised
29 September 2014
Accepted
20 October 2014

BACKGROUND AND PURPOSE

4-Phenylquinolin-2(1*H*)-one (4-PQ) derivatives can induce cancer cell apoptosis. Additional new 4-PQ analogs were investigated as more effective, less toxic antitumour agents.

EXPERIMENTAL APPROACH

Forty-five 6,7,8-substituted 4-substituted benzyloxyquinolin-2(1*H*)-one derivatives were synthesized. Antiproliferative activities were evaluated using a 3-(4,5-dimethylthiazol-2-yl)-2,5-diphenyltetrazoliun bromide assay and structure–activity relationship correlations were established. Compounds **9b**, **9c**, **9e** and **11e** were also evaluated against the National Cancer Institute-60 human cancer cell line panel. Hoechst 33258 and Annexin V-FITC/PI staining assays were used to detect apoptosis, while inhibition of microtubule polymerization was assayed by fluorescence microscopy. Effects on the cell cycle were assessed by flow cytometry and on apoptosis-related proteins (active caspase-3, -8 and -9, procaspase-3, -8, -9, PARP, Bid, Bcl-xL and Bcl-2) by Western blotting.

KEY RESULTS

Nine 6,7,8-substituted 4-substituted benzyloxyquinolin-2(1*H*)-one derivatives (**7e**, **8e**, **9b**, **9c**, **9e**, **10c**, **10e**, **11c** and **11e**) displayed high potency against HL-60, Hep3B, H460, and COLO 205 cancer cells (IC_{50} < 1 μM) without affecting Detroit 551 normal human cells (IC_{50} > 50 μM). Particularly, compound **11e** exhibited nanomolar potency against COLO 205 cancer cells. Mechanistic studies indicated that compound **11e** disrupted microtubule assembly and induced G2/M arrest, polyploidy and apoptosis via the intrinsic and extrinsic signalling pathways. Activation of JNK could play a role in TRAIL-induced COLO 205 apoptosis.

CONCLUSION AND IMPLICATIONS

New quinolone derivatives were identified as potential pro-apoptotic agents. Compound **11e** could be a promising lead compound for future antitumour agent development.

Abbreviations

4-PQ, 4-phenylquinolin-2(1*H*)-one; AGT, alkylguanine-DNA alkyltransferase; BG, benzylguanine; CDK, cyclin dependent kinase; NCI, National Cancer Institute; PPA, polyphosphoric acid; SAR, structure–activity relationship

Tables of Links

TARGETS	
Enzymes[a]	**Catalytic receptors**[b]
Aurora A kinase	DR4, death receptor 4
Aurora B kinase	DR5, death receptor 5
CDK1, cyclin dependent kinase 1	Fas
ERK1/2	TNFR1, TNF receptor 1
JNK	TRAF2, TNF receptor-associated factor 2
p38	Tubulin
RIP, receptor interacting protein (kinase)	

LIGANDS
Bid
Colchicine
TNFα
TRAIL

These Tables list key protein targets and ligands in this article which are hyperlinked to corresponding entries in http://www.guidetopharmacology.org, the common portal for data from the IUPHAR/BPS Guide to PHARMACOLOGY (Pawson *et al.*, 2014) and are permanently archived in the Concise Guide to PHARMACOLOGY 2013/14 ([a,b]Alexander *et al.*, 2013a,b).

Introduction

Cancer is presently a worldwide health problem and the leading cause of death in the United States and other developed countries (Rastogi *et al.*, 2004). Cancer is a formidable disease caused by disordered cell growth and invasion of tissues and organs. While various therapies and strategies have been developed to treat cancer, most of them have limitations. Thus, new anticancer drugs are continually needed. The main challenge facing clinical cancer therapy is to find a specific approach that kills malignant cells with no or few adverse effects on normal tissues and considerable attempts have been made to develop innovative, safe and effective methods to defeat cancer. While scientists have discovered many agents with cytostatic action against cancer cells (Liu *et al.*, 2007; Folger *et al.*, 2011), increasing understanding of the biological processes involved in cancer cell survival has led to the design and discovery of better targeted, novel therapeutic anticancer drugs. For several chemotherapeutic agents, a direct correlation has been found between antitumour efficacy and ability to induce apoptosis (Kaufmann and Earnshaw, 2000). Thus, approaches aimed at promoting apoptosis in cancer cells have gained importance in cancer research (Fesik, 2005; Fischer and Schulze-Osthoff, 2005).

Heterobicycles are indispensable structural units in compounds with a broad range of biological activities. Among various nitrogen-containing fused heterocyclic skeletons, quinoline and quinolone structures are important components prevalent in a vast array of biological systems. Compounds with a quinoline nucleus exhibit various pharmacological properties, including antioxidant (Chung and Woo, 2001; Zhang *et al.*, 2013), anti-inflammatory (Baba *et al.*, 1996; Mukherjee and Pal, 2013), antibacterial (Cheng *et al.*, 2013), anti-human immunodeficiency virus (Freeman *et al.*, 2004; Hopkins *et al.*, 2004), antimalarial (Cornut *et al.*, 2013; Pandey *et al.*, 2013), antituberculosis (Lilienkampf *et al.*, 2009), anti-Alzheimer's disease (Fiorito *et al.*, 2013), anticancer (Wang *et al.*, 2011; Abonia *et al.*, 2012; Chan *et al.*, 2012) activities. Accordingly, Solomon and Lee described quinoline-containing subunits as 'privileged structures' for drug development (Solomon and Lee, 2011). 2-Quinolone [quinolin-2(1*H*)-one], also called 1-aza coumarin or carbostyril, and 4-quinolone are structural isomers. The 2-quinolone skeleton is a fertile source of biologically active compounds, including a wide spectrum of alkaloids investigated for antitumour activity (Ito *et al.*, 2004; He *et al.*, 2005; Nakashima *et al.*, 2012). In our previous investigation, 6,7-methylenedioxy-4-substituted phenylquinolin-2(1*H*)-one derivatives (4-phenylquinolin-2(1*H*)-ones; 4-PQs) were identified as novel apoptosis-inducing agents (Figure 1) (Chen *et al.*, 2013b). Recently, Arya and Agarwal reported that 4-hydroxyquinolin-2(1*H*)-one derivatives, prepared efficiently through microwave irradiation, showed strong photo-antiproliferative activity (Arya and Agarwal, 2007). Thus, we have directed our focus onto 4-PQ analogues as inducers of apoptosis. In our current study, we targeted the 2-quinolone structure as a basic scaffold of new derivatives with different substituents.

Purine-based compounds such as olomoucine and roscovitine (Figure 1), which contain other heterobicyclic ring systems, are known ATP-binding site competitive inhibitors

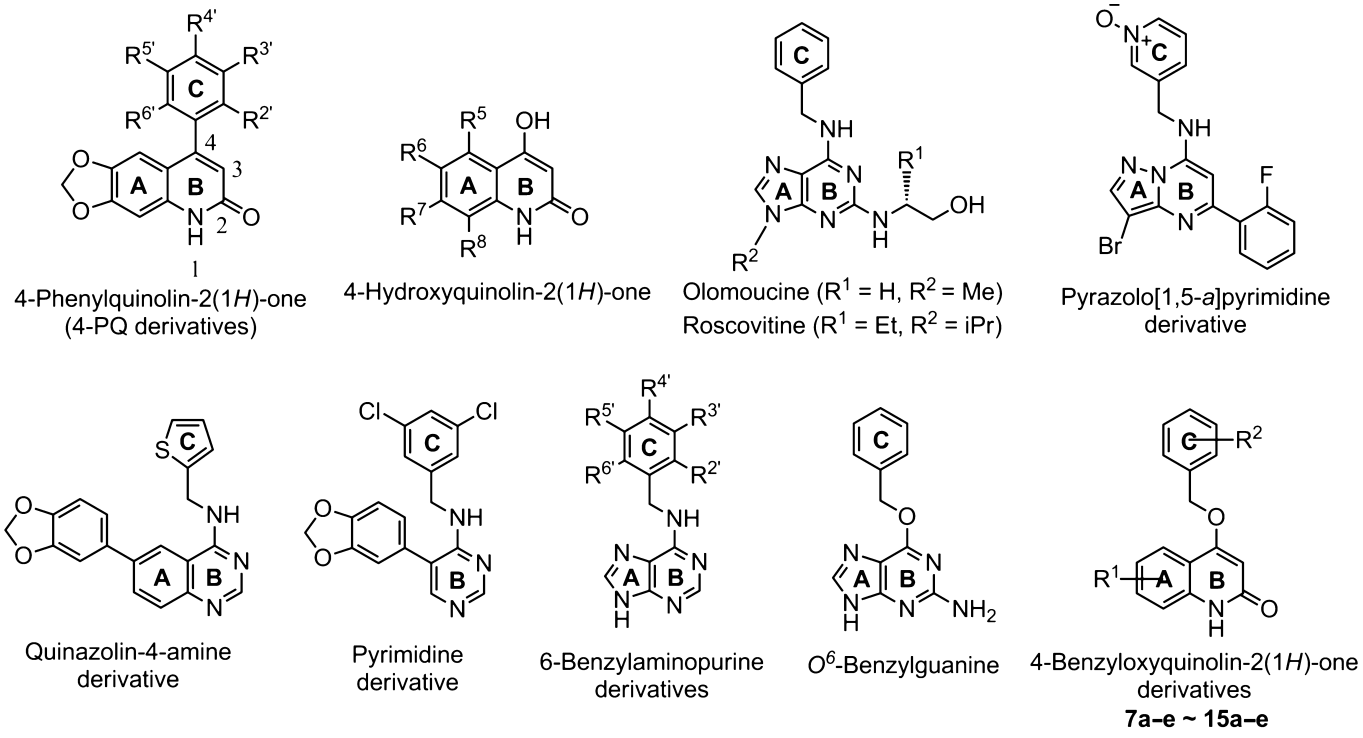

Figure 1

The structures of some anticancer agents and the general structure of the target compounds (**7a–e** ~ **15a–e**).

of cyclin dependent kinase (CDK) and are useful cell proliferation inhibitors in the treatment of cancer (Jorda *et al.*, 2011). Structure–activity relationship (SAR) studies on CDK inhibitors demonstrated that a small hydrophobic group such as a non-polar benzyl group at the O^6- or N^6-position of the heterobicycle maximized CDK inhibition (Gibson *et al.*, 2002; Zatloukal *et al.*, 2013). In addition, numerous CDK inhibitor-related compounds that contain benzyl or aryl methyl groups on different core scaffolds, such as pyrazolo[1,5-*a*]pyrimidines (Paruch *et al.*, 2007), quinazolin-4-amines (Mott *et al.*, 2009), pyrimidine (Coombs *et al.*, 2013) and aminopurine (Doležal *et al.*, 2006) (Figure 1), have been studied. Furthermore, a series of 6-(benzyloxy)-2-(aryldiazenyl)-9*H*-purine derivatives were reported to act as prodrugs of O^6-benzylguanine (O^6-BG; Figure 1), which selectively targets O^6-alkylguanine-DNA alkyltransferase (AGT) in hypoxic tumour cells (Zhu *et al.*, 2013). The AGT protein plays a critical role in DNA repair, which can be exploited in chemotherapeutic treatment of neoplastic cells (Dolan and Pegg, 1997; Daniels *et al.*, 2000). Alkylation of AGT with the benzyl group of O^6-BG results in complete depletion of the alkyltransferase protein. Consequently, numerous O^6-BG analogs have been developed as AGT inhibitors (Chae *et al.*, 1995; Terashima and Kohda, 1998). Ruiz *et al.* (2008) reported that a family of quinolinone compounds acted as novel non-nucleosidic AGT inhibitors. These quinolinones could reach the critical catalytic residue Cys^{145} buried deep within the binding groove, occupy the catalytic cleft of human DNA repair AGT protein and act as substrate mimics of the O^6-guanine moiety.

Furthermore, the activity of biologically proven anticancer pharmacophores can be enhanced by introducing appropriate substitutions on the chemical scaffolds. In medicinal chemistry, shortening or lengthening chain length is a useful tactic to improve the affinity of target binding. Some reports have demonstrated that the pro-apoptotic (anti-tumour) activity of certain compounds was dramatically improved by slightly changing the length and spacing of lateral branches, such as benzyl and other alkyl-aromatic side chains, on core skeletons (Al-Obaid *et al.*, 2009; Font *et al.*, 2011). Such exploration and utilization of chemical diversity relative to pharmacological space is an ongoing drug discovery strategy, referred to as privileged-substructure-based diversity-oriented synthesis (Oh and Park, 2011). Based on this strategy, as well as the structures shown in Figure 1, we proposed addition of a substituted benzyl (C ring) side chain linked at the O^4-position of 4-hydroxyquinolin-2(1*H*)-one (2-quinolone scaffold) as a possible strategy for discovering new leads with pro-apoptotic bioactivity. The flexibility of the benzyl moiety might provide better antitumour activity compared with our earlier 4-PQ derivatives (Figure 1). Therefore, we designed a series of 4-benzyloxyquinolin-2(1*H*)-one analogues **7a–e** ~ **15a–e**, with the general structures of target compounds depicted in Figure 1. To the best of our knowledge, this is the first evaluation of 2-quinolone analogues bearing an O^4-benzyl moiety against cancer. The goal of the current study was to discover more effective and less toxic antitumour agents and contribute to the SAR profile of 2-quinolones with anti-proliferative activity and pro-apoptotic activities in cancer cells.

Methods

Materials and physical measurements

All solvents and reagents were obtained commercially and used without further purification. The progress of all reactions was monitored by TLC on 2 × 6 cm pre-coated silica gel 60 F_{254} plates of thickness 0.25 mm (Merck KGaA, Darmstadt, Germany). The chromatograms were visualized under UV at 254–366 nm. Column chromatography was performed using silica gel 60 (Merck KGaA, particle size 0.063–0.200 mm). Melting points (mp) were determined with a Yanaco MP-500D melting point apparatus (Yanaco New Science Inc., Kyoto, Japan) and are uncorrected. IR spectra were recorded on Shimadzu IR-Prestige-21 spectrophotometers (Shimadzu Corp., Kyoto, Japan) as KBr pellets. The one-dimensional NMR (^{1}H and ^{13}C) spectra were obtained on a Bruker Avance DPX-200 FT-NMR spectrometer (Bruker Corp., Billerica, MA, USA) at room temperature. The two-dimensional NMR spectra were obtained on a Bruker Avance DPX-400 FT-NMR spectrometer (Bruker Corp.) and chemical shifts were expressed in parts per million (ppm, δ). The following abbreviations are used: s, singlet; d, doublet; t, triplet; dd, double doublet and m, multiplet. Mass spectra were performed at the Instrument Center of National Science Council at National Chung Hsing University (Taichung City, Taiwan) using a Finnigan ThermoQuest MAT 95 XL (EI-MS) (Thermo Fisher Scientific Inc., Waltham, MA, USA).

General procedure for the synthesis of 4-hydroxyquinolin-2(1H)-one derivatives (**5a–i**)

4-Hydroxyquinolin-2(1*H*)-one derivatives **5a–i** were prepared by 'one-pot' cyclization in polyphosphoric acid (PPA). A mixture of the appropriate substituted aniline **1a–i** (1 equiv) and diethylmalonate (**2**) (1.2 equiv) was heated with PPA (five to six times by weight) at 130°C for 2–6 h (TLC monitoring). Then, the mixture was cooled and diluted with water. A gum solidified upon standing overnight and the precipitate was filtered, washed with water and air-dried to provide **5a–i** with sufficient purity for the next reaction. Physical and spectroscopic data for **5a** are given in the succeeding text; the data for the remaining compounds are provided as Supporting Information.

4-Hydroxyquinolin-2(1H)-one (**5a**) (Mohamed, 1991; Nadaraj et al., 2006; Arya and Agarwal, 2007; Park et al., 2007; Zhang et al., 2008)

Compound **5a** (3.48 g, 21.59 mmol) was obtained from aniline (**1a**) (3.82 g, 41.01 mmol) and diethylmalonate (**2**) (7.88 g, 49.20 mmol); yield: 53%; light-yellow solid; mp: 276–278°C; IR (KBr) ν (cm^{-1}): 1660 (C = O); ^{1}H NMR (200 MHz, DMSO-d_6) δ (ppm): 5.77 (s, 1H, H–3), 7.12 (t, J = 7.5 Hz, 1H, H–6), 7.26 (d, J = 8.2 Hz, 1H, H–8), 7.47 (t, J = 7.8 Hz, 1H, H–7), 7.77 (d, J = 8.0 Hz, 1H, H–5), 11.28 (br. s, 1H, NH); ^{13}C NMR (50 MHz, DMSO-d_6) δ (ppm): 98.56, 115.48, 115.63, 121.61, 123.11, 131.33, 139.55, 163.05, 164.18; MS (EI, 70 eV) *m/z*: 161.1[M]$^+$; HRMS (EI) *m/z*: calculated for $C_9H_7NO_2$: 161.0477; found: 161.0472.

General procedure for the synthesis of 6,7,8-substituted 4-substituted benyloxyquinolin-2(1H)-one derivatives (**7a–e**, **8a–e**, **9a–e**, **10a–e**, **11a–e**, **12a–e**, **13a–e**, **14a–e**, **15a–e**)

A mixture of 4-hydroxyquinolin-2(1*H*)-one derivatives **5a–i** (1 equiv) and K_2CO_3 (2 equiv) in DMF (10–20 mL) was heated at 90°C for 1–2 h. The appropriate benzyl chloride or bromide (**6a–e**, 1–1.4 equiv) was added and the mixture was heated at 80–90°C for 1–6 h. Reaction completion was confirmed by TLC monitoring. The mixture was poured into ice water (200 mL) and the precipitated solid was collected by filtration and then washed with water. The residue was treated with ethyl acetate (EtOAc) and purified by recrystallization. If no solid was formed after the addition of ice water, then the reaction mixture was extracted with EtOAc (3 × 100 mL). The combined organic layers were dried over anhydrous $MgSO_4$ before evaporation of solvent *in vacuo*. The residue was isolated by column chromatography (silica gel, EtOAc as eluate) and then recrystallized to give the corresponding pure products, 4-benzyloxyquinolin-2(1*H*)-one derivatives **7a–e**, **8a–e**, **9a–e**, **10a–e**, **11a–e**, **12a–e**, **13a–e**, **14a–e** and **15a–e**. Physical and spectroscopic data for **11e** are given as examples; the data for the remaining compounds are provided as Supporting Information.

4-(3′,5′-Dimethoxybenzyloxy)-6-methoxyquinolin-2(1H)-one (**11e**)

Compound **11e** (0.70 g, 2.05 mmol) was obtained from **5e** (1.12 g, 5.86 mmol) and 3,5-dimethoxybenzyl bromide (1.48 g, 6.40 mmol); yield: 35%; white crystal; mp: 217–219°C; IR (KBr) ν (cm^{-1}): 1674 (C = O); ^{1}H NMR (200 MHz, DMSO-d_6) δ (ppm): 3.74 (s, 6H, 3′, 5′–OCH_3), 3.76 (s, 3H, 6–OCH_3), 5.20 (s, 2H, –O–CH_2–), 5.94 (s, 1H, H–3), 6.47 (dd, J = 2.2,2.2 Hz, 1H, H–4′), 6.66 (d, J = 2.2 Hz, 2H, H–2′, H–6′), 7.14–7.26 (m, 3H, H–5,7,8), 11.32 (br. s, 1H, NH); ^{13}C NMR (50 MHz, DMSO-d_6) δ (ppm): 55.63 (2C), 55.78, 70.05, 98.71, 100.04, 104.17, 105.62 (2C), 115.50, 117.18, 120.50, 133.55, 138.76, 154.43, 161.07 (2C), 161.89, 163.23; MS (EI, 70 eV) *m/z*: 341.0 [M]$^+$; HRMS (EI) *m/z*: calculated for $C_{19}H_{19}NO_5$: 341.1263; found: 341.1257.

3-(4,5-dimethylthiazol-2-yl)-2,5-diphenyltetrazoliun bromide (MTT) assay for antiproliferative activity

Human tumour cell lines (HTCLs) of the cancer screening panel were maintained in RPMI-1640 medium supplemented with 10% FBS (GIBCO®, Life Technologies, Grand Island, NY, USA), penicillin (100 U·mL^{-1})/streptomycin (100 μg·mL^{-1}) (GIBCO, Life Technologies) and 1% L-glutamine (GIBCO, Life Technologies) at 37°C in a humidified atmosphere containing 5% CO_2. Human hepatoma Hep 3B and normal skin Detroit 551 cells were maintained in DMEM medium supplemented with 10% FBS (GIBCO, Life Technologies), penicillin (100 U·mL^{-1})/streptomycin (100 μg·mL^{-1}) (GIBCO, Life Technologies) and 1% L-glutamine (GIBCO, Life Technologies) at 37°C in a humidified atmosphere containing 5% CO_2. Logarithmically growing cancer cells were used for all experiments. The HTCLs were treated with vehicle or test compounds for 48 h. Cell growth rate was determined by MTT reduction

assay (Mosmann, 1983). After 48 h treatment, cell growth rate was measured on an ELISA reader at a wavelength of 570 nm and the IC_{50} values of test compounds were calculated.

In vitro *National Cancer Institute (NCI)-60 HTCL panel*

In vitro cytotoxic activities were evaluated through the Developmental Therapeutic Program (DTP) of the NCI (Shoemaker, 2006). For more information on the anticancer screening protocol, please see: http://dtp.nci.nih.gov/branches/btb/ivclsp.html.

Cell morphology and Hoechst 33258 staining

COLO 205 cells were plated at a density of 2.5×10^5 cells per well in 12-well plates and then incubated with 50 nM of compound **11e** for 12 to 48 h. Cells were directly examined and photographed under a contrast-phase microscope. Nuclei were stained with Hoechst 33258 (bis-benzimide; Sigma-Aldrich, St. Louis, MO, USA) to detect chromatin condensation or nuclear fragmentation, features of apoptosis. After 0, 12, 24, 36 and 48 h, **11e**-treated cells were stained with 5 $\mu g \cdot mL^{-1}$ Hoechst 33258 for 10 min. After washing twice with PBS, cells were fixed with 4% paraformaldehyde (PFA) in PBS for 10 min at 25°C. Fluorescence of the soluble DNA (apoptotic) fragments was measured in a Leica DMIL Inverted Microscope (Leica Microsystems GmbH, Wetzlar, Germany) at an excitation wavelength of 365 nm and emission wavelength of 460 nm.

Apoptosis studies

Determination of apoptotic cells by fluorescent staining was carried out as described previously (van Engeland *et al.*, 1998; Zhuang *et al.*, 2013). The Annexin V-FITC Apoptosis Detection Kit was obtained from Strong Biotech Corporation (Taipei, Taiwan). The COLO 205 cells (2×10^5 cells·per well) were fluorescently labelled for detection of apoptotic and necrotic cells by adding 100 µL of binding buffer, 2 µL of Annexin V-FITC and 2 µL of propidium iodide (PI) to each sample. Samples were mixed gently and incubated at room temperature in the dark for 15 min. Binding buffer (300 µL) was added to each sample immediately before flow cytometric analysis. A minimum of 10 000 cells within the gated region was analysed.

Flow cytometric analysis for cell cycle

Compound **11e** (final concentration 50 nM) was added to COLO 205 cells for 0, 12, 24, 36 and 48 h. Cells were fixed in 70% EtOH overnight, washed twice and resuspended in PBS containing 20 $\mu g \cdot mL^{-1}$ PI, 0.2 $mg \cdot mL^{-1}$ RNase A and 0.1% Triton X-100 in the dark. After 30 min incubation at 37°C, cell cycle distribution was analysed using ModFit LT Software (Verity Software House, Topsham, ME, USA) in a BD FACSCanto flow cytometer (Becton Dickinson, San Jose, CA, USA).

Molecular modelling

The crystal structure of microtubules in complex with *N*-deacetyl-*N*-(2-mercaptoacetyl)-colchicine (DAMA-colchicine) was downloaded from the Protein Data Bank (PDB entry 1SA0: http://www.rcsb.org/pdb/home/home.do) (Ravelli *et al.*, 2004). Docking studies were performed for proposed **11e** in the colchicine-binding site of tubulin. The AutoDock Vina (The Scripps Research Institute, Molecular Graphics Lab., La Jolla, CA, USA) was used to perform docking calculations (Trott and Olson, 2010). The final results were prepared with PyMOL (v. 1.3) (Schrödinger LLC., Shanghai Office, Shanghai, China) in Windows 7. After removing the ligand and solvent molecules, hydrogen atoms were added to each amino acid atom. The three-dimensional structure of compound were obtained from ChemBioDraw ultra 12.0 (PerkinElmer Inc., Waltham, MA, USA) followed by MM2 energy minimization. Docking was carried out by AutoDock Vina in the colchicine-binding pocket. Grid map in AutoDock 4.0 was used to define the interaction of protein and ligand in the binding pocket. For compound binding into the colchicine-binding site, a grid box size of $25 \times 25 \times 25$ points in x, y and z directions was built and the grid centre was located in x = 116.909, y = 89.688 and z = 7.904.

Localization of microtubules

After treatment, cells were fixed with 4% PFA in PBS, blocked with 2% BSA, stained with anti-tubulin monoclonal antibody, and then with FITC conjugated anti-mouse IgG antibody. PI was used to stain the nuclei. Cells were visualized using a Leica TCS SP2 Spectral Confocal System (Leica Microsystems GmbH).

Mitochondrial membrane potential analysis

Cells were plated (6 well plates) at 1.0×10^6 cells·per well and treated with 50 nM **11e** for 6–24 h. Mitochondrial membranes were stained with 0.5 mL JC-1 working solution (BD MitoScreen Kit; BD Biosciences Pharmingen, San Diego, CA, USA) added to each sample. Samples were incubated for 10–15 min at 37°C in the dark. Mitochondrial membrane potential was measured using the BD FACSCanto flow cytometer (Becton Dickinson).

Western blot assay

The treated cells (1×10^7 cells·10 mL^{-1} in 10 cm dish) were collected and washed with PBS. After centrifugation, cells were lysed in a lysis buffer. The lysates were incubated on ice for 30 min and centrifuged at 12 000 *g* for 20 min. Supernatants were collected and protein concentrations were then determined using the Bradford assay. After adding a 5 × sample loading buffer containing 625 mM Tris-HCl, pH = 6.8, 500 mM dithiothreitol, 10% SDS, 0.06% bromophenol blue and 50% glycerol, protein samples were separated by electrophoresis on 10% SDS-polyacrylamide gel and transferred to a nitrocellulose membrane. Immunoreactivity was detected using the Western blot chemiluminescence reagent system (PerkinElmer, Boston, MA, USA).

Statistical analysis

Statistical analysis was performed with ANOVA followed by Tukey's test. All data were expressed as mean ± SEM. $P < 0.001$ was indicative of a significant difference.

Results

Chemistry

The synthetic procedures for the new 4-substituted benzyloxyquinolin-2(1*H*)-ones (**7a–e ~ 15a–e**) are illustrated

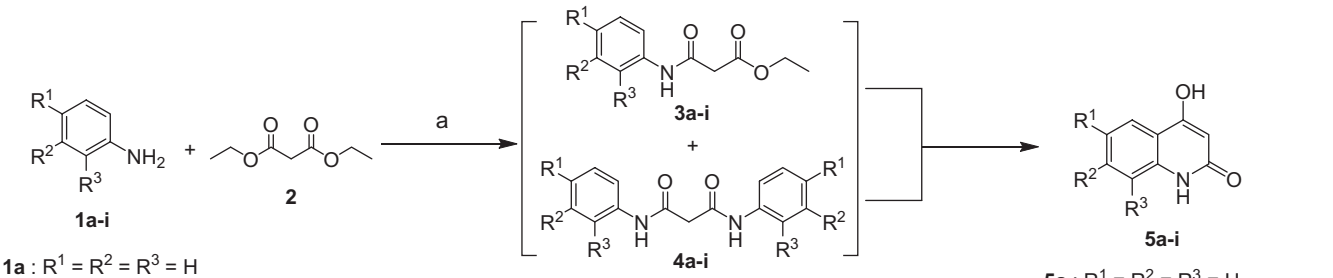

1a : $R^1 = R^2 = R^3 = H$
1b : $R^1 = F$, $R^2 = R^3 = H$
1c : $R^1 = Cl$, $R^2 = R^3 = H$
1d : $R^1 = CH_3$, $R^2 = R^3 = H$
1e : $R^1 = OCH_3$, $R^2 = R^3 = H$
1f : $R^1 = R^3 = H$, $R^2 = OCH_3$
1g : $R^1 = R^2 = H$, $R^3 = OCH_3$
1h : $R^1 = R^2 = H$, $R^3 = Cl$
1i : $R^1 = R^2 = H$, $R^3 = CH_3$

3a, **4a** : $R^1 = R^2 = R^3 = H$
3b, **4b** : $R^1 = F$, $R^2 = R^3 = H$
3c, **4c** : $R^1 = Cl$, $R^2 = R^3 = H$
3d, **4d** : $R^1 = CH_3$, $R^2 = R^3 = H$
3e, **4e** : $R^1 = OCH_3$, $R^2 = R^3 = H$
3f, **4f** : $R^1 = R^3 = H$, $R^2 = OCH_3$
3g, **4g** : $R^1 = R^2 = H$, $R^3 = OCH_3$
3h, **4h** : $R^1 = R^2 = H$, $R^3 = Cl$
3i, **4i** : $R^1 = R^2 = H$, $R^3 = CH_3$

5a : $R^1 = R^2 = R^3 = H$
5b : $R^1 = F$, $R^2 = R^3 = H$
5c : $R^1 = Cl$, $R^2 = R^3 = H$
5d : $R^1 = CH_3$, $R^2 = R^3 = H$
5e : $R^1 = OCH_3$, $R^2 = R^3 = H$
5f : $R^1 = R^3 = H$, $R^2 = OCH_3$
5g : $R^1 = R^2 = H$, $R^3 = OCH_3$
5h : $R^1 = R^2 = H$, $R^3 = Cl$
5i : $R^1 = R^2 = H$, $R^3 = CH_3$

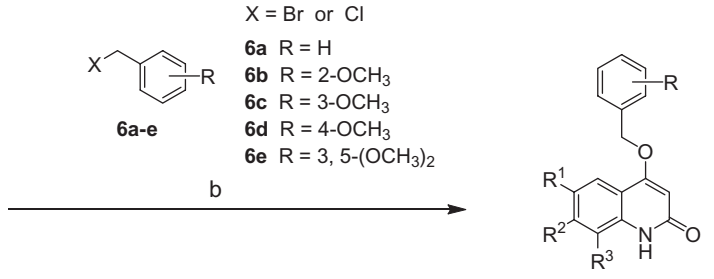

7a : $R^1 = R^2 = R^3 = H$; R = H
7b : $R^1 = R^2 = R^3 = H$; R = 2'-OCH_3
7c : $R^1 = R^2 = R^3 = H$; R = 3'-OCH_3
7d : $R^1 = R^2 = R^3 = H$; R = 4'-OCH_3
7e : $R^1 = R^2 = R^3 = H$; R = 3', 5'-$(OCH_3)_2$

8a : $R^1 = F$, $R^2 = R^3 = H$; R = H
8b : $R^1 = F$, $R^2 = R^3 = H$; R = 2'-OCH_3
8c : $R^1 = F$, $R^2 = R^3 = H$; R = 3'-OCH_3
8d : $R^1 = F$, $R^2 = R^3 = H$; R = 4'-OCH_3
8e : $R^1 = F$, $R^2 = R^3 = H$; R = 3', 5'-$(OCH_3)_2$

9a : $R^1 = Cl$, $R^2 = R^3 = H$; R = H
9b : $R^1 = Cl$, $R^2 = R^3 = H$; R = 2'-OCH_3
9c : $R^1 = Cl$, $R^2 = R^3 = H$; R = 3'-OCH_3
9d : $R^1 = Cl$, $R^2 = R^3 = H$; R = 4'-OCH_3
9e : $R^1 = Cl$, $R^2 = R^3 = H$; R = 3', 5'-$(OCH_3)_2$

10a : $R^1 = CH_3$, $R^2 = R^3 = H$; R = H
10b : $R^1 = CH_3$, $R^2 = R^3 = H$; R = 2'-OCH_3
10c : $R^1 = CH_3$, $R^2 = R^3 = H$; R = 3'-OCH_3
10d : $R^1 = CH_3$, $R^2 = R^3 = H$; R = 4'-OCH_3
10e : $R^1 = CH_3$, $R^2 = R^3 = H$; R = 3', 5'-$(OCH_3)_2$

11a : $R^1 = OCH_3$, $R^2 = R^3 = H$; R = H
11b : $R^1 = OCH_3$, $R^2 = R^3 = H$; R = 2'-OCH_3
11c : $R^1 = OCH_3$, $R^2 = R^3 = H$; R = 3'-OCH_3
11d : $R^1 = OCH_3$, $R^2 = R^3 = H$; R = 4'-OCH_3
11e : $R^1 = OCH_3$, $R^2 = R^3 = H$; R = 3', 5'-$(OCH_3)_2$

12a : $R^1 = R^3 = H$, $R^2 = OCH_3$; R = H
12b : $R^1 = R^3 = H$, $R^2 = OCH_3$; R = 2'-OCH_3
12c : $R^1 = R^3 = H$, $R^2 = OCH_3$; R = 3'-OCH_3
12d : $R^1 = R^3 = H$, $R^2 = OCH_3$; R = 4'-OCH_3
12e : $R^1 = R^3 = H$, $R^2 = OCH_3$; R = 3', 5'-$(OCH_3)_2$

13a : $R^1 = R^2 = H$, $R^3 = OCH_3$; R = H
13b : $R^1 = R^2 = H$, $R^3 = OCH_3$; R = 2'-OCH_3
13c : $R^1 = R^2 = H$, $R^3 = OCH_3$; R = 3'-OCH_3
13d : $R^1 = R^2 = H$, $R^3 = OCH_3$; R = 4'-OCH_3
13e : $R^1 = R^2 = H$, $R^3 = OCH_3$; R = 3', 5'-$(OCH_3)_2$

14a : $R^1 = R^2 = H$, $R^3 = Cl$; R = H
14b : $R^1 = R^2 = H$, $R^3 = Cl$; R = 2'-OCH_3
14c : $R^1 = R^2 = H$, $R^3 = Cl$; R = 3'-OCH_3
14d : $R^1 = R^2 = H$, $R^3 = Cl$; R = 4'-OCH_3
14e : $R^1 = R^2 = H$, $R^3 = Cl$; R = 3', 5'-$(OCH_3)_2$

15a : $R^1 = R^2 = H$, $R^3 = CH_3$; R = H
15b : $R^1 = R^2 = H$, $R^3 = CH_3$; R = 2'-OCH_3
15c : $R^1 = R^2 = H$, $R^3 = CH_3$; R = 3'-OCH_3
15d : $R^1 = R^2 = H$, $R^3 = CH_3$; R = 4'-OCH_3
15e : $R^1 = R^2 = H$, $R^3 = CH_3$; R = 3', 5'-$(OCH_3)_2$

Scheme 1

Reagents and conditions: (A) 130°C with PPA. (B) K_2CO_3/DMF, 80–90°C.

in Scheme 1. A general synthetic approach to the key intermediate 4-hydroxyquinolin-2(1*H*)-one is the Knorr quinoline synthesis, which involves cyclization and dehydration of a transient β-ketoanilide, formed by condensation of a β-keto ester and aniline at relatively high temperature. More specific synthetic approaches include cyclization of *N*-acetylanthranilic acid derivatives (Buckle *et al.*, 1975), condensation of malonates/malonic acid with anilines using $ZnCl_2$ and $POCl_3$ (Zhang *et al.*, 2008; Priya *et al.*, 2010), Ph_2O (Ahvale *et al.*, 2008) and cyclization of malonodianilides with PPA (Cai *et al.*, 1996; Park *et al.*, 2007; Moradi-e-Rufchahi, 2010), CH_3SO_3H/P_2O_5 (Kappe *et al.*, 1988) and *p*-toluenesulfonic acid (Nadaraj *et al.*, 2006). In our study, 4-hydroxyquinolin-2(1*H*)-one derivatives (**5a–i**) were synthe-

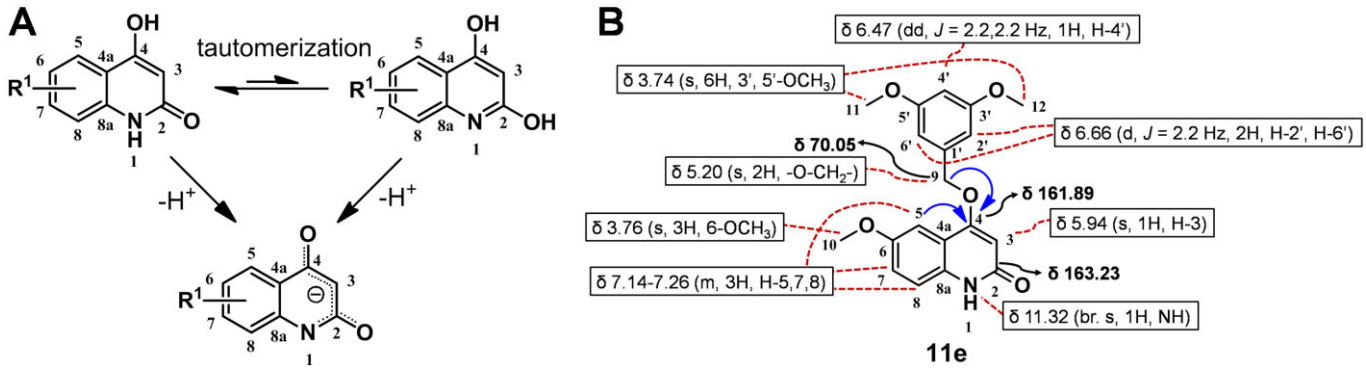

Figure 2

Alkylation of 4-hydroxyquinolin-2(1*H*)-ones. (A) Tautomerism of 4-hydroxyquinolin-2(1*H*)-one derivatives. (B) Key HMBC correlations (blue arrows) of **11e** indicated alkylation at the 4-OH position.

sized by treatment of a substituted aniline (**1a–i**) with diethylmalonate (**2**) in one flask (Mohamed, 1991; Arya and Agarwal, 2007), followed by cyclization of the formed monoanilide (**3a–i**) or malondianilide (**4a–i**) precursors in the presence of PPA. The target 4-benzyloxyquinolin-2(1*H*)-one derivatives **7a–e**, **8a–e**, **9a–e**, **10a–e**, **11a–e**, **12a–e**, **13a–e**, **14a–e** and **15a–e** were synthesized by reaction of the intermediate 4-hydroxyquinolin-2(1*H*)-one derivatives **5a–i** with various benzyl halide **6a–e** in the presence of K_2CO_3 and DMF (Guo *et al.*, 2009; Deng *et al.*, 2010). All synthetic products were characterized by IR, ^{1}H and ^{13}C NMR and mass spectroscopy.

The 2-quinolones have a minor tautomeric structure (2-hydroxyquinoline) because of protonation of the carbonyl oxygen (Lewis *et al.*, 1991). Deprotonation of the 2-quinolone would cause ring resonance and electron shifting within the *N*-1, *O*-2, *C*-3 and *O*-4 positions of the 4-hydroxyquinolin-2(1*H*)-one derivatives (Figure 2A) (Pirrung and Blume, 1999). Consequently, earlier reports have indicated that 4-hydroxyquinolin-2(1*H*)-ones could be alkylated at the 1-*N*H, 2-*O*H, 4-*O*H or 3-*C*H position (Park and Lee, 2004; Ahmed *et al.*, 2010; 2011). Therefore, we confirmed the structures of our synthesized compounds using NMR spectroscopic analyses. The ^{1}H NMR spectrum of 4-benzyloxyquinolin-2(1*H*)-one derivatives **7a–e ~ 15a–e** featured a singlet for *O*-linked C(9)-H_2 methylene protons between 5.13 and 5.27 ppm, a singlet for a C(3)-*H* proton between 5.80 and 6.09 ppm and a broad singlet for an exchangeable N*H* group between 10.47 and 11.54 ppm. The chemical shifts for the benzylic CH_2 were consistent with *O*-alkylation rather than *N*-alkylation (Park and Lee, 2004). The ^{13}C shifts for *O*-alkylated compounds are typically downfield (higher ppm value; 52.7–68.4) compared with *N*-alkylated compounds (lower ppm value; 28.6–45.0) (LaPlante *et al.*, 2013). The ^{13}C NMR spectra of **7a–e ~ 15a–e** included an *O*-linked methylene carbon between 65.74 and 70.74 ppm, which again indicated *O*-alkylation. Furthermore, regioselective alkylation at the 4-*O*H position was confirmed by two-dimensional NMR study via heteronuclear multiple-quantum correlation and heteronuclear multiple-bond correlation (HMBC) spectroscopy experiments that disclose the relationship between ^{1}H and ^{13}C coupling. In the case of compound **11e**, as shown in Figure 2B, the 4-*O*-linkage was supported by observation of ^{3}*J*-HMBC correlations between C(9)-*H* methylene protons (δ_H 5.20) on the 3′,5′-dimethoxybenzyloxy moiety with the carbon at *C*(4) position (δ_c 161.89) of the 2-quinolone core, which shows a further correlation with the C(5)-*H* proton (δ_H 7.14–7.26, overlapped). In other words, O^4-alkylation was determined through the observation of H9/C4 and H5/C4 cross-peaks. These data proved that 3′,5′-dimethoxybenzyloxy moiety is attached to the 4-*O*-position of the 2-quinolone core structure. Furthermore, the IR spectra of **7a–e ~ 15a–e** possessed a characteristic absorption band for an amido C = O group (1633–1674 cm^{-1}).

Biological evaluation and SAR analysis

All newly synthesized target compounds (**7a–e**, **8a–e**, **9a–e**, **10a–e**, **11a–e**, **12a–e**, **13a–e**, **14a–e** and **15a–e**) were assayed for growth inhibitory activity against Detroit 551 cells (human normal skin fibroblast) and four cancer cell lines – HL-60 (leukaemia), Hep 3B (hepatoma), H460 (non-small-cell lung carcinoma) and COLO 205 (colorectal adenocarcinoma). Cells were treated with compounds for 48 h and cell proliferation was determined by MTT assay. The antiproliferative activity of each compound was presented as the concentration of compound that achieved 50% inhibition (IC_{50}) of cancer cell growth. The results are summarized in Table 1. Collectively, the present series of novel 4-benzyloxyquinolin-2(1*H*)-one derivatives exhibited a range of potencies against the four tested tumour cell lines. Among them, compounds **7e**, **8e**, **9b**, **9c**, **9e**, **10c**, **10e**, **11c** and **11e** displayed high potency against HL-60, Hep3B, H460 and COLO 205 cells, with IC_{50} value less than 1 μM (Table 1). Notably, **11e** displayed the most prominent growth inhibitory activities against these four cell lines with IC_{50} values ranging from 14 to 40 nM. Moreover, none of the active compounds showed cytotoxicity (IC_{50} > 50 μM) towards Detroit 551 cells. These results suggested that this new series of 4-benzyloxyquinolin-2(1*H*)-one derivatives could effectively suppress tumour growth without causing toxicity to normal somatic cells.

Based on the biological data obtained so far, SAR correlations were determined. Firstly, we evaluated the effects of

Table 1

Antiproliferative effects of compounds **7a–e** ~ **15a–e**

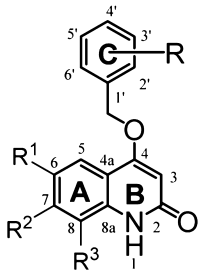

Compound	R^1	R^2	R^3	R	IC_{50} (μM)[a] HL-60[b]	Hep 3B[b]	H460[b]	COLO205[b]	Detroit 551[b]
7a	H	H	H	H	>50	>50	>50	>50	>50
7b	H	H	H	2′-OCH_3	>50	>50	>50	>50	>50
7c	H	H	H	3′-OCH_3	16.4	>50	>50	7.5	>50
7d	H	H	H	4′-OCH_3	>50	>50	>50	>50	>50
7e	H	H	H	3′, 5′-$(OCH_3)_2$	0.68	0.64	0.69	0.42	>50
8a	F	H	H	H	>50	>50	>50	>50	>50
8b	F	H	H	2′-OCH_3	8.7	>50	>50	7.3	>50
8c	F	H	H	3′-OCH_3	>50	>50	>50	50	>50
8d	F	H	H	4′-OCH_3	>50	>50	>50	>50	>50
8e	F	H	H	3′, 5′-$(OCH_3)_2$	0.4	0.9	0.6	0.39	>50
9a	Cl	H	H	H	4.5	>50	>50	9.8	>50
9b	Cl	H	H	2′-OCH_3	0.6	2.2	2.8	0.41	>50
9c	Cl	H	H	3′-OCH_3	0.3	0.8	1.0	0.35	>50
9d	Cl	H	H	4′-OCH_3	>50	>50	>50	>50	>50
9e	Cl	H	H	3′, 5′-$(OCH_3)_2$	0.0295	0.15	0.19	0.054	>50
10a	CH_3	H	H	H	–	>50	>50	8.2	–
10b	CH_3	H	H	2′-OCH_3	–	1.8	1.7	1.0	–
10c	CH_3	H	H	3′-OCH_3	–	0.68	0.89	0.36	–
10d	CH_3	H	H	4′-OCH_3	–	>50	>50	>50	–
10e	CH_3	H	H	3′, 5′-$(OCH_3)_2$	–	0.54	0.27	0.06	–
11a	OCH_3	H	H	H	8.5	27.0	51.7	8.8	>50
11b	OCH_3	H	H	2′-OCH_3	1.5	4.3	3.3	5.0	>50
11c	OCH_3	H	H	3′-OCH_3	0.2	0.9	0.6	0.21	>50
11d	OCH_3	H	H	4′-OCH_3	>50	>50	>50	>50	>50
11e	OCH_3	H	H	3′, 5′-$(OCH_3)_2$	0.014	0.035	0.04	0.028	>50
12a	H	OCH_3	H	H	–	9.55	17.3	14.2	–
12b	H	OCH_3	H	2′-OCH_3	–	4.02	7.1	6.4	–
12c	H	OCH_3	H	3′-OCH_3	–	3.23	>50	8.2	–
12d	H	OCH_3	H	4′-OCH_3	–	>50	>50	>50	–
12e	H	OCH_3	H	3′, 5′-$(OCH_3)_2$	–	2.11	3.96	4.9	–
13a	H	H	OCH_3	H	>50	>50	>50	34.1	>50
13b	H	H	OCH_3	2′-OCH_3	>50	>50	>50	>50	>50
13c	H	H	OCH_3	3′-OCH_3	20.0	39.9	32.3	22.6	>50
13d	H	H	OCH_3	4′-OCH_3	>50	>50	>50	>50	>50
13e	H	H	OCH_3	3′, 5′-$(OCH_3)_2$	3.3	3.8	2.2	2.6	>50
14a	H	H	Cl	H	–	>50	>50	>50	–
14b	H	H	Cl	2′-OCH_3	–	>50	>50	>50	–
14c	H	H	Cl	3′-OCH_3	–	>50	>50	>50	–
14d	H	H	Cl	4′-OCH_3	–	>50	>50	>50	–
14e	H	H	Cl	3′, 5′-$(OCH_3)_2$	–	3.64	19.4	9.7	–
15a	H	H	CH_3	H	>50	>50	>50	>50	>50
15b	H	H	CH_3	2′-OCH_3	20.0	>50	>50	41.5	>50
15c	H	H	CH_3	3′-OCH_3	>50	>50	>50	>50	>50
15d	H	H	CH_3	4′-OCH_3	10.0	>50	>50	>50	>50
15e	H	H	CH_3	3′, 5′-$(OCH_3)_2$	0.72	2.0	3.3	2.6	>50
Etoposide					5.48	–	1.0	–	–

[a]Human tumour cells were treated with different concentrations of samples for 48 h. Data are presented as IC_{50} (μM, the concentration of 50% proliferation-inhibitory effect). [b]Cell lines include leukaemia (HL-60), liver carcinoma (Hep3B), lung carcinoma (H460), colon carcinoma (COLO205) and normal skin fibroblasts (Detroit 551).

methoxy substitution of the *C*-4 benzyloxy ring (C ring) on the cytotoxic activity. Generally, compounds with 3′,5′-dimethoxybenzyloxy side chain (**7e–15e**) showed the highest potency in their respective series (**7–15**). Among them, compounds **7e**, **8e**, **9e**, **10e** and **11e** exhibited significant activity against Hep 3B, H460 and COLO 205 cancer cell lines (IC_{50} < 1 μM). These results indicated 3′,5′-dimethoxybenzyloxy substitution is preferred relative to other benzyl substitution. Compounds **9b**, **9c**, **10b**, **10c**, **11b**, **11c** with a 2′- or 3′-methoxybenzyloxy side chain demonstrated moderate activity (IC_{50} 0.2–5.0 μM), whereas compounds bearing side chains of benzyloxy or 4′-methoxybenzyloxy were inactive (IC_{50} > 50 μM) or exhibited only marginal activity (IC_{50} 4.5–10 μM).

Next, we explored the SAR of the 2-quinolone A ring. Compounds with a substituted benzyloxy moiety at *C*-4 and various functional groups at *C*-6, -7 and -8 were studied and different anticancer effects were found. Regarding the *C*-6 substitution, compound **8e** (6-fluoro), **9e** (6-chloro), **10e** (6-methyl) and **11e** (6-methoxy) were more potent than **7e** (no substitution). Moreover, compound **11e** (IC_{50} 0.014–0.04 μM) displayed the strongest growth inhibitory activity among the *C*-6 substituted compounds, suggesting that the *C*-6 methoxy group might play a pivotal role. Moving the methoxy group from *C*-6 to *C*-7 (**12e**, IC_{50} 2.11–4.9 μM) or *C*-8 (**13e**, IC_{50} 2.2–3.8 μM) dramatically decreased inhibitory activity. Activity also decreased when the *C*-8 methoxy of **13e** was replaced with chlorine (**14e**), while activity was retained when the methoxy was replaced with methyl (**15e**). Thus, in this series of 4-benzyloxy-2-quinolones, optimal antiproliferative effects were found with a 6-methoxy group on the 2-quinolone ring.

In the present work, the earlier findings can be summarized in the following two SAR conclusions:

(i) The *in vitro* anticancer activity of the substituted benzyloxy moiety (C ring) on the 4-position of 2-quinolone derivatives can be ranked in the following order of decreasing activity: 3′,5′-dimethoxybenzyloxy (**7e–15e**) > 3′-methoxybenzyloxy (**7c–15c**) ≧ 2′-methoxybenzyloxy (**7b–15b**) > benzyloxy (**7a–15a**) ≧ 4′-methoxybenzyloxy (**7d–15d**).

(ii) C-6 substituents on the 2-quinolone (A ring) resulted in better activity compared with C-7 and C-8 substituent. The following rank order of *in vitro* anticancer activity was found relative to the identity of the C-6 substituent: 6-methoxy > 6-chloro ≧ 6-methyl > 6-fluoro ≧ no substitution.

*Anticancer drug screen panel of compound **9b**, **9c**, **9e** and **11e** against NCI-60 human cancer cell lines*

We selected four potent compounds **9b**, **9c**, **9e** and **11e** and submitted them for screening against the NCI-60 HTCL panel assay through the US NCI DTP (Boyd and Paull, 1995; Shoemaker, 2006). The cell lines used in this assay represent nine tumour subpanels, leukaemia, melanoma and cancers of lung, colon, brain (CNS), ovary, kidney, prostate and breast. Initially, the compounds were added at a single dose (10 μM) and the culture was incubated for 48 h. End-point determinations were made with a sulforhodamine B assay. Results for each compound are given in Table 2, with a negative value in the cell growth percentage indicating an antiproliferative effect against that cell line. Compound **9b** displayed positive cytotoxic effects towards 11 out of 60 cell lines, and the positive cytotoxic proportions of **9c**, **9e** and **11e** were 10/59, 18/60 and 26/57. Our prominent compound **11e** exhibited inhibitory effects ranging from –59% to –0.80%. At the primary single high dose 10 μM (10^{-5} M), **9b**, **9c**, **9e** and **11e** showed greatest effects against colon carcinoma COLO 205 with cell growth percentage of –55, –57, –64 and –59 respectively. The melanoma MDA-MB-435 cell line was also sensitive to these compounds (growth percentages –46%, –43%, –43% and –41% respectively).

At the second evaluation stage, the selected compounds were evaluated at five different concentrations (0.01, 0.1, 1, 10 and 100 μM) against the same NCI-60 HTCL panel. The outcomes were represented by three calculated response parameters (GI_{50}, TGI and LC_{50}) for each cell line through growth percentage inhibition curves (Holbeck, 2004; Holbeck *et al.*, 2010). The GI_{50} value (growth inhibitory activity) corresponds to the concentration of compound causing 50% decrease in net cell growth, the TGI value (cytostatic activity) is the concentration of compound resulting in total growth inhibition (100% growth inhibition) and LC_{50} value (cytotoxic activity) is the lethal dose of compound causing net 50% death of initial cells. The calculated results are presented as log concentration (given in the Supporting Information), as shown in Table 3. The NCI data revealed broad-spectrum sensitivity profiles for **9b**, **9c**, **9e** and **11e** towards all nine cancer subpanels with GI_{50} values less than 1 μM, and less than 0.01 μM (log GI_{50} < –8.0) against some cell lines for **9e** and **11e**. The anticancer effects of these compounds were comparable with those of fluorouracil (5-FU), which is widely used clinically for treating cancer (Longley *et al.*, 2003). These screening results were in good agreement with the single dose results, showing broad anticancer spectra for **9b**, **9c**, **9e** and **11e**. Notably, compound **11e** exhibited GI_{50} values ranging from 0.01 to 8.08 μM in 51 of the 56 cell lines, with GI_{50} values below 0.01 μM in five cell lines (leukaemia K-562 and SR, non-small-cell lung cancer NCI-H522, colon cancer COLO 205, melanoma MDA-MB-435).

To further determine which cancer subtypes were more sensitive to these 4-benzyloxy-2-quinolones, we calculated subpanel-selectivity ratios based upon GI_{50} values. The calculated results are shown in Table 4 and Figure 3. Selectivity ratios less than 3 were rated non-selective, ratios ranging from 3 to 6 were termed moderately selective and ratios greater than 6 were designated highly selective (Boyd and Paull, 1995; Noolvi *et al.*, 2012; Chen *et al.*, 2013a). With all ratios less than 3, compounds **9b** and **9c** were rated non-selective towards all nine subpanels. Interestingly, both **9e** and **11e**, which contain a 3′,5′-dimethoxybenzyloxy moiety, were much more selective than **9b** and **9c** (Figure 3). As shown in Table 4, the average selectivity ratios of **9e** and **11e** (ratios = 6.51 and 4.05) were higher than those of **9b** and **9c** (ratios = 1.12 and 1.28). Compound **9e** exhibited selectivity against leukaemia, colon cancer, CNS cancer, melanoma, renal cancer and prostate cancer. In terms of the total MID (an average sensitivity across all cell lines), compound **11e** displayed significant activity (0.31 μM) and was moderately

Table 2

Growth percentages of selected compounds in the NCI *in vitro* 60-cell Drug Screen Program

	Compounds/Growth percentage (%)[a]			
Panel/Cell line	**9b**	**9c**	**9e**	**11e**
Leukaemia				
CCRF-CEM	18.56	11.98	15.94	**–26.21**[b]
HL-60(TB)	9.64	**–9.34**	7.37	**–32.61**
K-562	15.80	17.65	11.80	3.56
MOLT-4	39.79	38.04	42.35	4.78
RPMI-8226	19.77	17.87	15.90	**–6.67**
SR	14.68	5.97	7.02	**–4.86**
Non-small-cell lung cancer				
A549/ATCC	29.44	21.67	**–22.24**	7.15
EKVX	50.93	41.72	52.28	–
HOP-62	**–18.38**	**–22.55**	**–27.19**	24.70
HOP-92	19.45	46.83	43.66	28.92
NCI-H226	42.44	48.35	8.57	54.52
NCI-H23	32.69	33.31	3.47	**–47.65**
NCI-H322M	36.63	35.35	39.53	21.59
NCI-H460	10.03	5.68	2.71	3.87
NCI-H522	18.21	22.30	**–0.77**	**–29.70**
Colon cancer				
COLO 205	**–55.40**	**–57.40**	**–64.41**	**–59.50**
HCC-2998	23.46	27.86	**–12.73**	**–32.77**
HCT-116	25.11	28.76	3.95	0.12
HCT-15	24.78	19.69	17.60	7.24
HT-29	7.13	2.57	0.32	**–27.36**
KM12	30.65	22.39	10.66	1.77
SW-620	12.10	21.07	20.17	10.28
CNS cancer				
SF-268	42.91	42.47	27.59	8.61
SF-295	6.76	9.92	**–2.30**	**–3.44**
SF-539	5.03	**–2.10**	**–35.52**	**–28.70**
SNB-19	28.95	30.82	19.73	48.02
SNB-75	**–22.87**	**–16.82**	**–42.27**	–
U251	16.38	18.14	**–21.80**	5.44
Melanoma				
LOX IMVI	14.48	17.90	2.15	**–6.75**
MALME-3M	45.00	31.84	32.02	55.33
M14	13.96	19.46	8.30	**–50.76**
MDA-MB-435	**–46.28**	**–43.14**	**–43.16**	**–41.44**
SK-MEL-2	23.93	5.30	10.59	**–14.08**
SK-MEL-28	**–12.04**	4.07	**–8.81**	7.02
SK-MEL-5	**–25.75**	**–32.70**	0.36	**–27.48**
UACC-257	24.32	21.96	19.86	34.86
UACC-62	**–19.98**	4.59	5.49	**–48.21**

Table 2

Continued

Panel/Cell line	Compounds/Growth percentage (%)[a]			
	9b	9c	9e	11e
Ovarian cancer				
IGROV1	45.21	39.68	46.14	–
OVCAR-3	4.64	6.22	**–59.96**	**–32.89**
OVCAR-4	34.25	42.73	29.48	40.39
OVCAR-5	48.30	36.30	32.38	18.06
OVCAR-8	33.86	24.06	6.15	9.94
NCI/ADR-RES	19.48	20.52	3.42	**–14.04**
SK-OV-3	**–17.68**	**–27.16**	**–27.00**	**–0.80**
Renal cancer				
786-0	33.73	39.62	3.94	**–2.61**
A498	21.88	16.02	**–2.40**	**–8.21**
ACHN	44.36	43.14	23.77	19.79
CAKI-1	31.23	30.29	27.34	9.52
RXF 393	**–14.00**	–	**–25.73**	**–11.48**
SN12C	27.70	32.18	16.82	2.52
TK-10	50.99	41.50	**–2.79**	18.32
UO-31	38.23	34.68	28.46	30.52
Prostate cancer				
PC-3	21.26	23.95	27.74	20.50
DU-145	16.06	14.85	20.65	1.31
Breast cancer				
MCF7	**–5.90**	1.34	**–35.96**	13.94
MDA-MB-231/ATCC	29.63	40.04	5.25	**–2.71**
HS 578T	9.12	21.68	21.06	31.90
BT-549	42.21	48.16	30.87	**–19.04**
T-47D	**–19.71**	**–16.85**	21.81	50.59
MDA-MB-468	24.05	**–25.33**	**–23.96**	**–4.24**
Mean growth	17.02	16.59	5.26	0.19
Range of growth	**–55.40** to 50.99	**–57.40** to 48.35	**–64.41** to 52.28	**–59.50** to 55.33
The most sensitive cell line	COLO 205 (Colon cancer)	COLO 205 (Colon cancer)	COLO 205 (Colon cancer)	COLO 205 (Colon cancer)
Positive cytostatic effect[c]	47/60	49/59	41/60	28/57
Positive cytotoxic effect[d]	11/60	10/59	18/60	26/57

[a]Data obtained from NCI *in vitro* 60-cell screen programme at 10 μM. [b]Negative values represent compound proved lethal to the cancer cell line (cell death). [c]Ratio between number of cell lines with percentage growth from 0 to 50 and total number of cell lines. [d]Ratio between number of cell lines with percentage growth of <0 and total number of cell lines. The bold values indicate significant cytotoxicity toward cancer cell lines.

selective towards the breast cancer subpanel and highly selective against leukaemia, colon cancer and prostate cancer. Among the subpanels rated highly selective, colon cancer was extremely sensitive to compound **11e** (NSC 764592; Figure 3). This compound showed exceptional potency against the individual cell line COLO 205 (LC_{50} 0.09 μM, TGI 0.03 μM) (Table 3). From the dose-response curves against six colon cancer cell lines (Figure 4), it is also obvious that **11e** exhibited particular selectivity against COLO 205.

*Morphological changes and apoptosis in COLO 205 cells induced by compound **11e***

Based on the *in vitro* cytotoxicity data, **11e** (NSC 764592), the most potent compound against COLO 205 cells was selected for further biological studies. Apoptosis is well known as a process of programmed cell death (Elmore, 2007). In our previous study, 4-phenyl-2-quinolone analogues (4-PQs) induced cell cycle arrest and apoptosis in both HL-60 and

Table 3

In vitro antitumour activity (GI_{50} in μM), toxicity (LC_{50} in μM) and TGI data of selected compounds **9b**, **9c**, **9e** and **11e**

	Compounds[a]														
	9b			**9c**			**9e**			**11e**			**5-FU**[b]		
Panel/Cell line	**GI_{50}**	**TGI**	**LC_{50}**	**GI_{50}**	**TGI**	**LC_{50}**	**GI_{50}**	**TGI**	**LC_{50}**	**GI_{50}**	**TGI**	**LC_{50}**	**GI_{50}**	**TGI**	**LC_{50}**
Leukaemia															
CCRF-CEM	0.39	19.50	>100	0.31	>100	>100	0.04	>100	>100	0.03	>100	>100	10.00	>100	>100
HL-60(TB)	–	–	–	–	–	–	–	–	–	0.04	>100	>100	2.51	>100	>100
K-562	0.08	11.60	92.50	0.03	–	>100	<**0.01**	1.67	>100	<**0.01**	>100	>100	3.98	>100	>100
MOLT-4	0.51	32.50	>100	0.33	>100	>100	0.05	>100	>100	0.07	>100	>100	0.32	50.12	>100
RPMI-8226	0.61	21.40	>100	0.43	>100	>100	0.08	>100	>100	0.03	>100	>100	0.05	50.12	>100
SR	0.20	0.89	>100	0.03	0.95	>100	<**0.01**	0.08	>100	<**0.01**	>100	>100	0.03	10.00	>100
Non-small-cell lung cancer															
A549/ATCC	–	–	–	–	–	–	–	–	–	0.02	>100	>100	0.20	63.10	>100
EKVX	0.46	40.70	>100	0.22	>100	>100	0.24	>100	>100	–	–	–	63.10	>100	>100
HOP-62	0.53	2.82	17.80	0.33	–	>100	0.04	14.10	43.30	0.03	12.20	75.10	0.40	>100	>100
HOP-92	1.09	5.18	31.80	1.42	>100	>100	11.90	>100	>100	0.02	10.80	>100	79.43	>100	>100
NCI-H226	2.24	41.00	>100	3.25	>100	>100	10.20	>100	>100	2.80	>100	>100	50.12	>100	>100
NCI-H23	0.93	12.00	69.40	0.51	>100	>100	0.08	63.80	>100	0.07	13.30	>100	0.32	39.81	>100
NCI-H322M	0.57	9.76	>100	0.36	>100	>100	0.05	>100	>100	0.08	>100	>100	0.20	7.94	>100
NCI-H460	0.39	3.87	37.10	0.05	–	>100	0.03	23.90	>100	0.03	>100	>100	0.06	50.12	>100
NCI-H522	0.15	0.46	6.55	0.03	0.19	12.30	<**0.01**	0.03	0.10	<**0.01**	0.03	>100	7.94	63.10	>100
Colon cancer															
COLO 205	0.39	2.45	60.80	0.22	1.89	>100	0.03	0.10	2.48	<**0.01**	0.03	0.09	0.16	63.10	>100
HCC-2998	1.04	12.40	61.10	0.30	>100	>100	0.12	31.60	>100	0.05	1.98	>100	0.05	39.81	>100
HCT-116	0.42	1.74	6.74	0.11	–	–	0.04	>100	>100	0.04	10.40	>100	0.25	3.98	25.12
HCT-15	0.54	>100	>100	0.29	>100	>100	0.04	>100	>100	0.03	18.90	>100	0.10	50.12	>100
HT-29	0.30	0.85	11.50	0.04	0.41	–	0.03	0.08	>100	0.01	–	>100	0.16	63.10	>100
KM12	0.53	18.10	>100	0.06	>100	>100	0.04	>100	>100	0.03	3.18	>100	0.20	39.81	>100
SW-620	0.39	12.50	>100	0.05	>100	>100	0.03	>100	>100	0.02	>100	>100	1.00	>100	>100
CNS cancer															
SF-268	0.68	20.60	>100	0.49	>100	>100	0.05	75.20	>100	1.08	>100	>100	1.58	>100	>100
SF-295	0.24	0.74	5.10	0.09	0.77	4.63	0.02	0.08	24.90	–	–	–	0.25	3.98	>100
SF-539	0.60	2.77	14.00	0.39	2.21	>100	0.04	1.20	>100	0.03	0.21	58.70	0.06	79.43	>100
SNB-19	0.58	14.30	>100	0.41	4.49	>100	0.06	28.30	>100	0.09	>100	>100	3.98	79.43	>100
SNB-75	0.30	1.40	14.80	0.24	0.95	13.50	0.03	0.09	36.90	0.01	0.05	26.70	79.43	>100	>100
U251	0.45	10.50	46.80	0.42	3.57	>100	0.05	16.00	56.60	0.04	12.00	>100	1.00	79.43	>100
Melanoma															
LOX IMVI	0.59	3.58	32.70	0.51	2.78	>100	0.07	>100	>100	0.06	10.30	>100	0.25	50.12	79.43
MALME-3M	0.32	10.30	>100	0.11	>100	>100	0.03	54.30	>100	–	>100	>100	0.05	2.51	>100
M14	0.32	1.11	57.90	0.14	1.25	>100	0.04	2.07	>100	0.04	0.26	4.29	1.00	>100	>100
MDA-MB-435	0.06	0.24	0.73	0.02	0.04	0.09	<**0.01**	0.02	0.08	<**0.01**	0.02	2.68	0.08	79.43	>100
SK-MEL-2	0.34	0.86	25.40	0.15	0.74	>100	0.02	0.06	27.20	–	>100	>100	63.10	>100	>100
SK-MEL-28	0.71	12.70	>100	0.47	>100	>100	0.07	>100	>100	0.07	>100	>100	1.00	63.10	>100
SK-MEL-5	0.26	–	54.70	0.19	–	>100	0.03	>100	>100	0.02	1.85	7.08	0.50	39.81	79.43
UACC-257	–	>100	>100	–	>100	>100	–	>100	>100	8.08	>100	>100	3.98	79.43	>100
UACC-62	0.45	4.25	30.80	0.35	8.90	>100	0.04	51.60	>100	0.03	>100	>100	0.50	39.81	>100

Table 3

Continued

	Compounds[a]														
	9b			9c			9e			11e			5-FU[b]		
Panel/Cell line	GI_{50}	TGI	LC_{50}	GI_{50}	TGI	LC_{50}	GI_{50}	TGI	LC_{50}	GI_{50}	TGI	LC_{50}	GI_{50}	TGI	LC_{50}
Ovarian cancer															
IGROV1	0.56	6.57	48.60	0.35	>100	>100	0.06	64.80	>100	0.42	>100	>100	1.26	31.62	>100
OVCAR-3	0.38	1.36	7.54	0.24	1.17	5.06	0.02	0.07	7.79	0.02	0.07	28.60	0.02	0.32	50.12
OVCAR-4	2.77	39.80	>100	0.96	>100	>100	0.83	>100	>100	1.11	>100	>100	3.98	79.43	>100
OVCAR-5	2.01	22.80	>100	1.90	>100	>100	0.32	>100	>100	0.09	69.50	>100	10.00	50.12	>100
OVCAR-8	0.48	13.20	57.00	0.43	>100	>100	0.06	28.30	>100	0.05	>100	>100	1.58	31.62	>100
NCI/ADR-RES	0.37	8.09	79.50	0.08	–	>100	0.03	11.70	>100	0.01	24.60	>100	0.32	12.59	>100
SK-OV-3	0.50	2.30	11.70	0.35	2.10	>100	0.03	1.04	96.90	0.03	0.93	64.20	19.95	63.10	>100
Renal cancer															
786-0	0.62	2.51	8.27	0.58	–	>100	0.07	32.30	>100	1.15	11.40	>100	0.79	50.12	>100
A498	0.45	1.87	6.10	0.16	1.88	>100	0.03	22.30	>100	0.02	0.09	78.10	0.40	>100	>100
ACHN	0.73	4.47	31.40	0.61	>100	>100	0.06	>100	>100	0.08	>100	>100	0.32	31.62	>100
CAKI-1	0.32	3.55	52.50	0.06	–	>100	0.03	>100	>100	0.02	>100	>100	0.08	2.00	>100
RXF 393	0.47	2.58	13.70	0.41	3.14	>100	0.05	0.31	36.30	0.02	0.08	>100	2.51	31.62	>100
SN12C	0.67	20.80	>100	0.67	>100	>100	0.10	>100	>100	0.09	>100	>100	0.50	25.12	>100
TK-10	–	–	–	–	–	–	–	–	–	1.05	75.80	>100	1.26	79.43	>100
UO-31	0.39	2.36	15.50	0.16	>100	>100	0.04	>100	>100	0.08	>100	>100	1.58	50.12	>100
Prostate cancer															
PC-3	0.89	24.10	>100	0.71	>100	>100	0.06	>100	>100	0.02	>100	>100	2.51	>100	>100
DU-145	0.56	13.70	>100	0.33	–	>100	0.04	29.30	>100	0.04	16.00	>100	0.40	>100	>100
Breast cancer															
MCF7	0.57	12.30	78.90	0.32	>100	>100	0.21	>100	>100	0.03	>100	>100	0.08	50.12	>100
MDA-MB-231/ATCC	0.92	10.10	58.50	1.29	>100	>100	0.15	55.50	>100	0.15	26.20	>100	6.31	39.81	>100
HS 578T	0.57	5.97	>100	0.30	2.89	>100	0.03	16.80	>100	0.02	100	>100	10.00	>100	>100
BT-549	0.74	19.60	>100	0.65	>100	>100	–	60.00	>100	0.20	9.26	>100	10.00	>100	>100
T-47D	0.51	7.23	38.20	0.38	>100	>100	–	>100	>100	0.04	>100	>100	7.94	50.12	>100
MDA-MB-468	1.73	6.13	29.70	0.29	1.03	>100	0.21	0.61	>100	0.05	0.41	>100	–	–	–

[a]Data obtained from NCI's *in vitro* disease-oriented human tumour cell lines screen. [b]NCI data for 5-FU: NSC 19893. (NCI Anticancer Screening Program; http://dtp.nci.nih.gov/docs/cancer/searches/standard_mechanism_list.html).

H460 cells (Chen *et al.*, 2013b). In order to characterize the cellular basis for the antiproliferative effects of the selected derivative **11e**, we investigated the ability of this compound to induce apoptosis in COLO 205 cells. Morphological analysis confirmed the cytotoxic effects of **11e** in COLO 205 cells. As shown in Figure 5A, the apoptotic morphological changes included cell rounding and shrinkage after 24 h incubation with 50 nM of **11e** (the black arrowhead indicates an apoptotic nucleus). To confirm the induction of apoptosis by **11e**, COLO 205 cells were stained with Hoechst 33258, a fluorescent DNA-staining dye, and cell morphology was investigated using fluorescence microscopy. As shown in Figure 5B, control cells exhibited uniformly dispersed chromatin, homogeneous blue fluorescence in the nuclei, normal organelles and intact cell membranes. In cells treated with 50 nM of **11e** for 24, 36 and 48 h, the nuclei budded off into several fragments and nuclear condensation and fragmentation were observed (Figure 5B), indicating typical characteristics of apoptosis, including condensation of chromatin, shrinkage of nuclei and appearance of apoptotic bodies (the black arrowhead indicates an apoptotic nucleus).

Annexin V-FITC/PI double-labelling was used to detect phosphatidylserine externalization, a characteristic effect of apoptosis (van Engeland *et al.*, 1998; Zhuang *et al.*, 2013). In Figure 5C, populations of viable (annexin V–, PI–), early apoptotic (annexin V+, PI–), late apoptotic (annexin V+ , PI+) and necrotic (annexin V–, PI+) cells are found in quadrants (Q) 3, 4, 2 and 1 respectively. Cells incubated in the absence of **11e** were undamaged and did not stain for annexin V-FITC and PI (Q3). After incubation with 50 nM of **11e**, the number of early apoptotic cells stained positive by annexin V-FITC and negative with PI (Q4) increased significantly with incubation time, from 5.5% (control) to 7.7% after 12 h, 12.7% after 24 h, 20.9% after 36 h and 21.8% after 48 h incubation. The

Table 4

Median growth inhibitory concentration (GI_{50}, μM) and GI_{50} selectivity ratios of selected compounds in the NCI *in vitro* 60-cell Drug Screen Program

	Compounds							
	9b (NSC 756950)		9c (NSC 756949)		9e (NSC 756951)		11e (NSC 764592)	
Subpanel tumour cell lines	**Subpanel MID[b] (μM)**	**Selectivity ratio[c]**	**Subpanel MID[b] (μM)**	**Selectivity ratio[c]**	**Subpanel MID[b] (μM)**	**Selectivity ratio[c]**	**Subpanel MID[b] (μM)**	**Selectivity ratio[c]**
Leukemia	0.36	1.74	0.23	1.86	0.06	7.56	0.04	7.36
Non-small cell lung cancer	0.80	0.79	0.77	0.55	3.22	0.13	0.44	0.72
Colon cancer	0.52	1.21	0.15	2.75	0.05	9.09	0.03	10.42
CNS cancer	0.48	1.31	0.34	1.24	0.04	10.28	0.25	1.25
Melanoma	0.38	1.64	0.24	1.73	0.04	10.00	1.38	0.23
Ovarian cancer	1.01	0.62	0.62	0.68	0.19	2.22	0.25	1.27
Renal cancer	0.52	1.20	0.38	1.11	0.05	7.89	0.31	1.00
Prostate cancer	0.73	0.86	0.52	0.81	0.05	8.57	0.03	10.42
Breast cancer	0.84	0.74	0.54	0.78	0.15	2.86	0.08	3.83
Total MID[a]	0.62		0.42		0.43		0.31	
Average selectivity Ratio		1.12		1.28		6.51		4.05

[a]Total MID = average sensitivity of all cell line in μM. [b]Subpanel MID = average sensitivity of individual subpanel cell lines in μM. [c]Selectivity ratio: Total MID[a]/Subpanel MID[b].

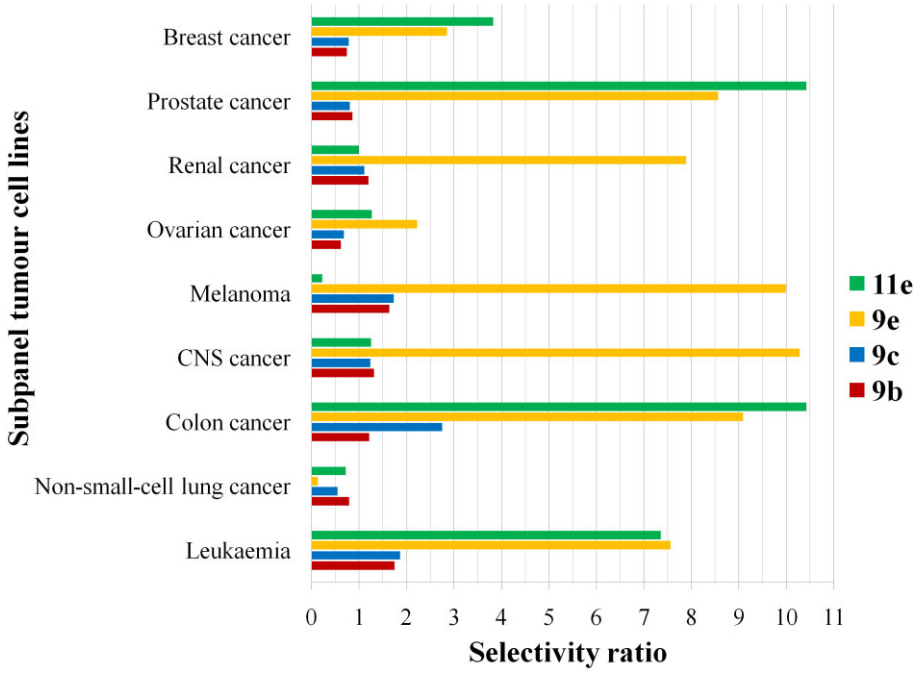

Figure 3
Subpanel tumour cell lines selectivity ratios of selected compounds **9b**, **9c**, **9e** and **11e**.

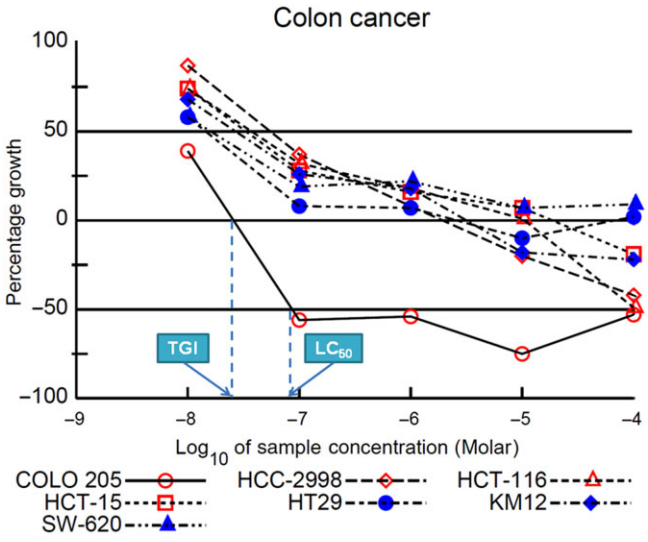

Figure 4
Dose-response curves of compound **11e** against colon cancer cell lines.

number of late apoptotic cells stained positive by annexin V-FITC and PI (Q2) also increased with incubation time, from 9.9% (control) to 10.2% after 12 h, 10.4% after 24 h, 8.6% after 36 h and 16.1% after 48 h incubation. Thus, when COLO 205 cells were stained with annexin-V/PI and analysed with flow cytometry, early and late apoptotic (annexin-V-stained) cells increased in a time-dependent manner (Figure 5C), which indicates that **11e** can induce apoptosis.

*Toxicity in COLO 205 cells induced by **11e***

Exposure of COLO 205 cells to **11e** for 48 h, followed by MTT metabolism assays, showed that **11e** reduced COLO 205 cell viability in a dose-dependent manner with an IC_{50} value of 27.2 ± 1.4 nM (Figure 6B). Inhibition of COLO 205 cell growth was also dependent of the time of exposure (24-72h) (Figure 6C).

***11e** induced apoptotic cell death and interfered with cell cycle distribution in G2/M phase arrest*

COLO 205 cells were treated with 50 nM of **11e** for 0, 6, 12, 24, 36 and 48 h, followed by flow cytometry analysis to determine the cell cycle distribution of treated cells, as well as to investigate the **11e**-induced inhibition of COLO 205 cell growth by cell cycle arrest and apoptotic mechanisms. As shown in Figure 7A, **11e** induced a time-dependent accumulation of cells at the G2/M phase.

***11e** inhibits microtubule polymerization in COLO 205 cells*

COLO 205 cells were treated with **11e** (50 nM) for 24 h and then visualized using confocal microscopy to investigate effects on microtubule function. As shown in Figure 7B, treatment with **11e** resulted in microtubule changes similar to those induced by colchicine. Both compounds caused cellular microtubule depolymerization with short microtubule fragments scattered throughout the cytoplasm. In contrast, another anti-cancer drug, taxol, significantly increased tubulin polymerization.

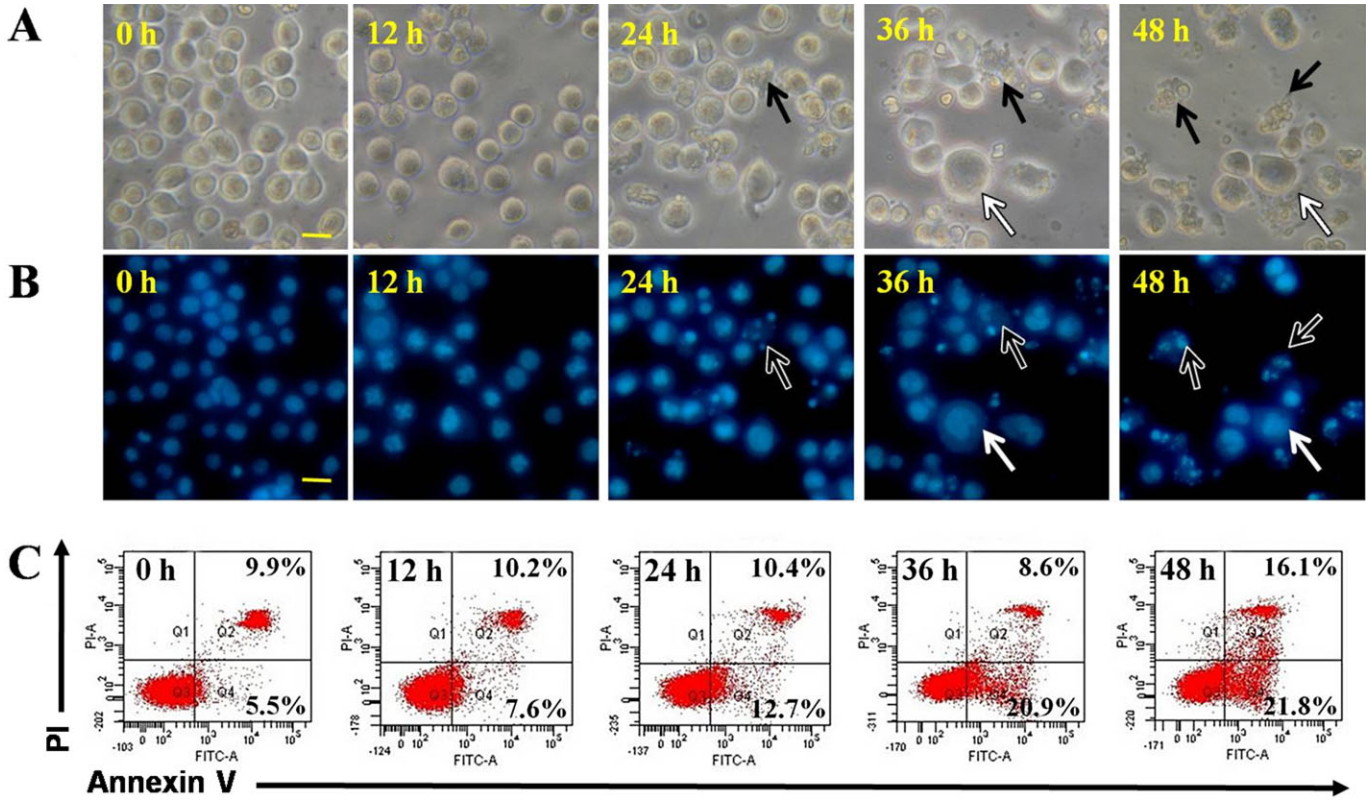

Figure 5

Compound **11e** induced time-dependent apoptosis in COLO 205 cells. COLO 205 cells were treated with 50 nM of **11e** for 0, 12, 24, 36 and 48 h. (A) Compound **11e** induced morphological changes in COLO 205 cells. (B) Fluorescent images of Hoechst staining showing **11e**-induced cell death. The black arrowhead indicates an apoptotic nucleus and the white arrowheads indicate multinucleate cells. (C) Apoptosis induced **by** compound **11e** was confirmed using annexin V/PI staining and flow cytometry. The fraction of annexin V-positive COLO 205 cells was 5.5% prior to treatment and 7.6%, 12.7%, 20.9% and 21.8% after treatment with **11e** for 12, 24, 36 and 48 h respectively. Scale bar = 20 μm.

Molecular modelling and computational studies

Using a molecular docking method and molecular mode of tubulin and DAMA-colchicine, **11e** was docked into the colchicine-binding domain of tubulin. As shown in Figure 8A and B, **11e** inserted deeply into the colchicine-binding pocket of α- and β-tubulin, very similar to the binding mode of DAMA-colchicine. Superimposition of compounds in the colchicine-binding site indicated that ring C and ring A are comparable pharmacophores between DAMA-colchicine and **11e** (Figure 8C and D). As shown in Figure 8D, the 1-NH group of **11e** overlapped with the acetamide-NH group of DAMA-colchicine. Moreover, the 1-NH of **11e** formed a hydrogen bond with $Thr^{179}\alpha$ as was also observed with the acetamide-NH group of DAMA-colchicine. The -O-CH_2- group of **11e** occupied a region in space in proximity to the C5 and C6 positions in the B-ring of DAMA-colchicine and was involved in hydrophobic interactions with $Lys^{254}\beta$, $Ala^{250}\beta$ and $Leu^{248}\beta$. The 3′,5′-dimethoxy of **11e** overlapped with the 1,3-dimethoxy moiety in the C ring of DAMA-colchicine, the C ring was involved in hydrophobic interactions with $Leu^{255}\beta$. Finally, the quinolin-2(1*H*)-one scaffold of **11e** partly overlapped with the A ring of DAMA-colchicine and formed hydrophobic interactions with $Asn^{258}\beta$ and $Lys^{352}\beta$.

***11e** changes the expression and phosphorylation status of G2/M regulatory proteins in COLO 205 cells*

Analysis of cell cycle-related protein expression explored the mechanisms by which **11e** induces G2/M arrest. Firstly, COLO 205 cells treated with 50 nM of **11e** showed increased cyclin B1 and CDK1 protein levels, which are markers for induction of mitotic arrest (Figure 9A). Secondly, given the importance of the aurora kinases in cancer cell mitosis and metastasis, the effects of **11e** (50 nM in COLO 205 cells) on aurora kinase function were investigated. As shown in Figure 9B, **11e** decreased aurora A, phospho-aurora A, aurora B and phospho-aurora B expression. Thirdly, we examined whether **11e** inhibited phosphorylation of histone H3 in COLO 205 cells. Histone H3 is a substrate for aurora B kinase. During mitosis, aurora B is required for phosphorylation of histone H3 on Ser^{10}, which might be important for chromosome condensation (Keen and Taylor, 2004). As shown by Western blot analysis, **11e** decreased phospho-H3 expression after a 6 h treatment (Figure 9B). This finding suggests that inactivation of aurora kinases A and B is involved in **11e**-induced G2/M arrest.

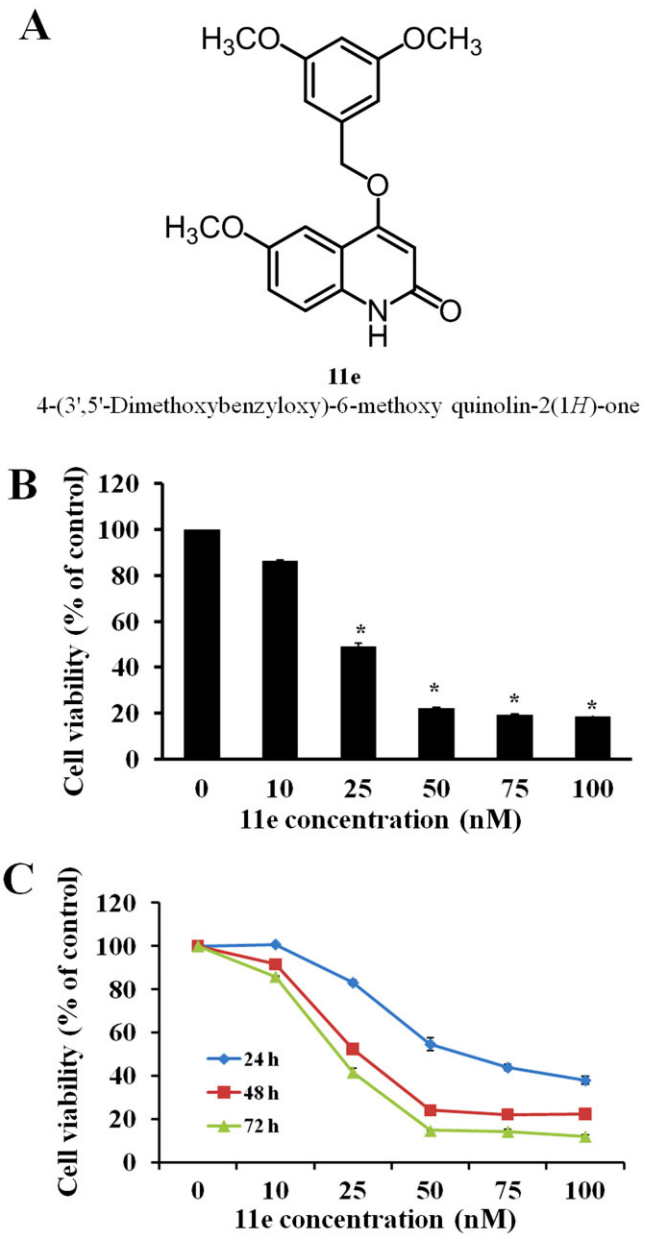

Figure 6

Effects of **11e** on the cytotoxicity of COLO 205 cells. (A) Chemical structure of **11e**. (B) COLO 205 cells were exposed to different concentrations of **11e** for 48 h. (C) COLO 205 cells were exposed to 0, 10, 25, 50, 75 and 100 nM **11e** for 24, 48 and 72 h. Cell viability was assessed using the MTT assay. The data are presented as mean ± SEM of three independent experiments. Cells without treatment served as a control. *$P < 0.001$ versus control.

11e-induced apoptosis associated with caspase-3, caspase-8, caspase-9 and PARP cleavage

To confirm the possibility that **11e**-induced apoptosis is related to activation of the intrinsic or extrinsic signalling pathway, COLO 205 cells were treated with 50 nM of **11e** for 6, 12, 24, 36 and 48 h, and then the activities of caspase-3, caspase-8 and caspase-9 were determined using a Western blot assay. As shown in Figure 10, **11e** induced significant caspase-3, caspase-8 and caspase-9 activity. Results from the Western blot assay also indicated that **11e** induced PARP cleavage, which is an important apoptosis marker. PARP is cleaved by caspase-3 between Asp^{214} and Gly^{215} to yield p85 and p25 fragments.

Intrinsic apoptotic pathway proteins are modulated during 11e-induced apoptosis

The mitochondria are key organelles in the control of apoptosis. Accordingly, we investigated whether **11e** was capable of inducing depolarization of the mitochondrial membrane potential ($\Delta\psi m$) using JC-1, a lipophilic fluorescent cation that incorporates into the mitochondrial membrane. COLO 205 cells were treated with 50 nM of **11e** for 6, 12, 24, 36 and 48 h, followed by staining with JC-1, to confirm apoptosis as the cause of decreased $\Delta\psi m$. As shown in Figure 11A, in healthy cells with high mitochondrial $\Delta\psi m$, JC-1 spontaneously formed complexes known as JC-1 polymer (P2), which showed intense red fluorescence (0 h). Over time, the percentage of cells with reduced red fluorescence (P3) showed a significant increase. This effect is indicative of a change in $\Delta\psi m$ in the population in which apoptosis was induced (6–36 h). Moreover, it is well known that the dissipation of $\Delta\psi m$ causes release of cytochrome *c*, Apaf-1, apoptosis-inducing factor (AIF) and Endo G into the cytosol, with consequent activation of the execution phase of apoptosis. In this study, we also demonstrated that mitochondrial cytochrome *c*, Apaf-1, AIF and Endo G were released into the cytosol during **11e**-induced apoptosis (Figure 11B).

Bcl-2 family proteins are key regulators of mitochondrial-related apoptotic pathways (Zhai *et al.*, 2008; Roy *et al.*, 2014). Some of these proteins, such as Bcl-2 and Bcl-xL, are anti-apoptotic (prosurvival) proteins, whereas others, such as Bad, Bax and Bid, are pro-apoptotic proteins. The Bcl-2 and Bcl-xL proteins are located in the outer mitochondrial membrane and are necessary for maintaining mitochondrial integrity. Furthermore, phosphorylation is a common characteristic of destabilized mitochondria. The balance of pro- and anti-apoptotic Bcl-2 proteins influences the sensitivity of cells to apoptotic stimuli (Brunelle and Letai, 2009). Previous research has shown that an increase in the ratio of Bax/Bcl-2 within a cell predisposes it to certain apoptotic stimuli. Bax and Bak induce the release of cytochrome *c* and loss of mitochondrial membrane potential, whereas Bcl-2 and Bcl-xL inhibit these effects. Because **11e** results in caspase-9 activation, which is also a mitochondria-mediated caspase, we sought to determine whether **11e** would affect the protein levels of these Bcl-2 family members. To confirm the involvement of Bcl-2 protein activity in **11e**-induced apoptosis, COLO 205 cells were treated with 50 nM of **11e** for 6, 12, 24, 36 and 48 h. As shown in Figure 11C, results indicated that **11e** reduced anti-apoptotic Bcl-2 and Bcl-xL levels and increased proapoptotic Bax and Bad levels, leading to changes in the Bax/Bcl-2 ratio and the release of cytochrome *c*, which in turn activates cleavage of caspase-9 and activation of caspase-3. These results demonstrate that **11e**-induced cell apoptosis involves the mitochondria-dependent pathway in COLO 205 cells.

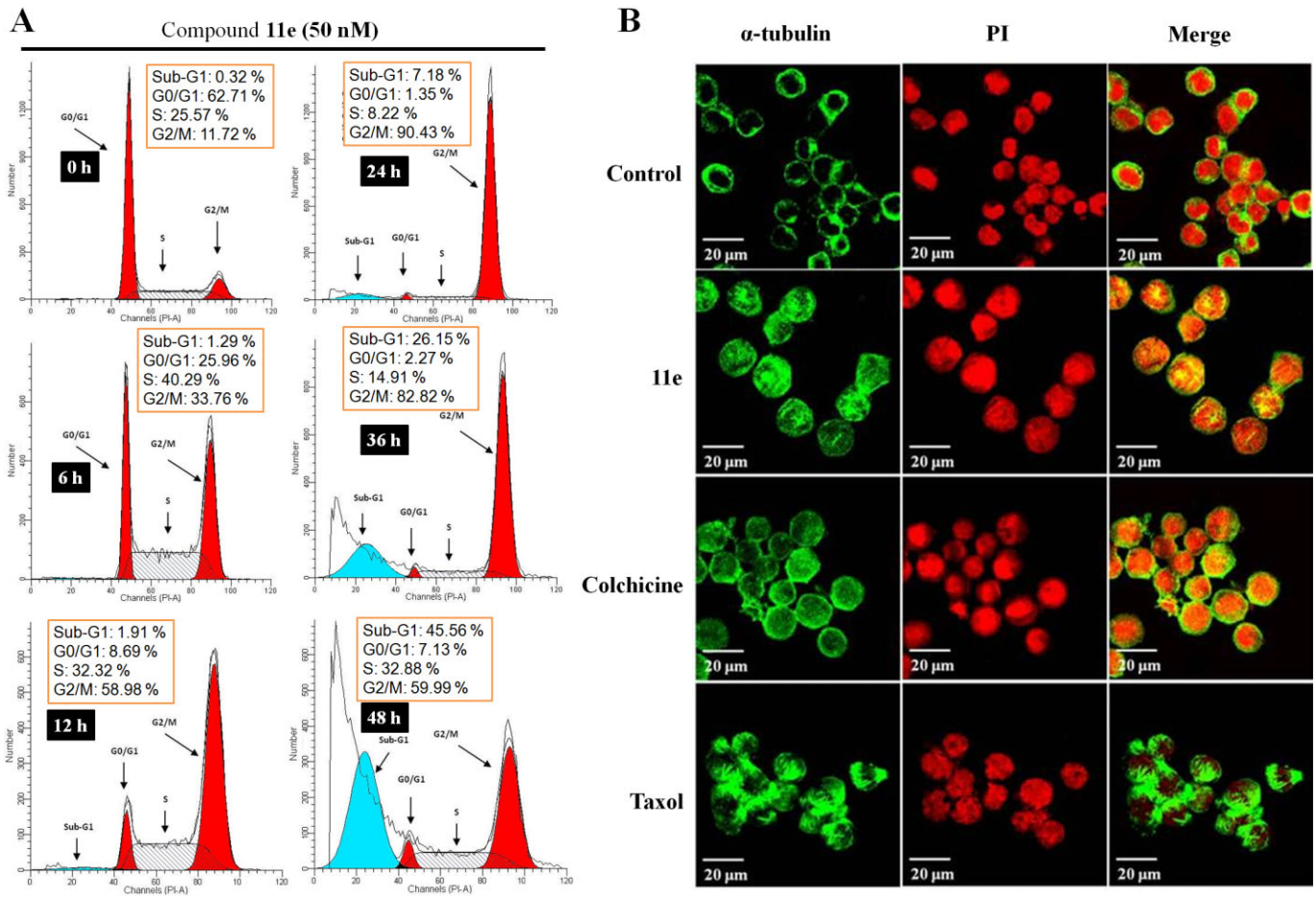

Figure 7

11e delays M phase progression and caused microtubule disassembly in cultured cells. (A) Flow cytometry analysis of cell cycle distribution in COLO 205 colon cancer cell line treated with 50 nM of **11e** for 0, 6, 12, 24, 36 and 48 h. (B) The effect of **11e** on the microtubule formation in COLO 205 cells. Cells were incubated with 0.1% DMSO, 50 nM **11e**, 1 μM colchicine or 1 μM taxol for 24 h. Immunofluorescence for α-tubulin (green) and PI nuclear staining (red). Cells were visualized using confocal microscopy.

*Effects of **11e** on death receptors and expression of their ligands*

Upon binding to their ligands, death receptors trigger apoptosis by stimulating caspase-8 mediated caspase cascades. In this study, expression of several death receptors (Fas, DR4 and DR5) and their ligands (FasL and TRAIL) were detected in COLO 205 cells (Figure 12). Compound **11e** treatment induced an increase in DR5, but did not alter Fas levels. These results suggest that DR5 up-regulation plays an important role in **11e**-mediated apoptosis through the extrinsic signalling pathways in COLO 205 cells.

***11e*-induced apoptosis is mediated via JNK signalling pathway**

MAPK respond to extracellular stimuli and regulate cellular activities, such as gene expression, mitosis, differentiation and cell survival/apoptosis. COLO 205 cells were treated with 50 nM of **11e** for 6, 12, 24, 36 and 48 h to investigate the effects of **11e** on ERK1/2, JNK and p38 signalling pathways. As shown in Figure 13, 11e decreased phospho-ERK1/2, p38 and phospho-p38 expression and induced JNK phosphorylation after 12 h incubation. These observations suggest that JNK activation is involved in **11e**-induced apoptosis.

Discussion and conclusion

In our continuing investigations of 4-PQ, new 4-benzyloxyquinolin-2(1*H*)-one derivatives (**7a–e** ~ **15a–e**) were designed and synthesized. In these novel molecules, the 2-quinolone central scaffold of 4-PQ is retained, but the linkage to the 4-phenyl aromatic ring has been extended by the addition of a CH_2O moiety, making a more flexible bridge. Nine compounds (**7e**, **8e**, **9b**, **9c**, **9e**, **10c**, **10e**, **11c** and **11e**) displayed high potency against HL-60, Hep3B, H460 and COLO 205 cells (IC_{50} < 1 μM) without affecting normal human Detroit 551 cells (IC_{50} > 50 μM). Among them, **11e** exhibited the highest potencies against these four tumour cell lines with IC_{50} values of 0.014, 0.035, 0.04 and 0.028 μM respectively. Notably, compound **11e**

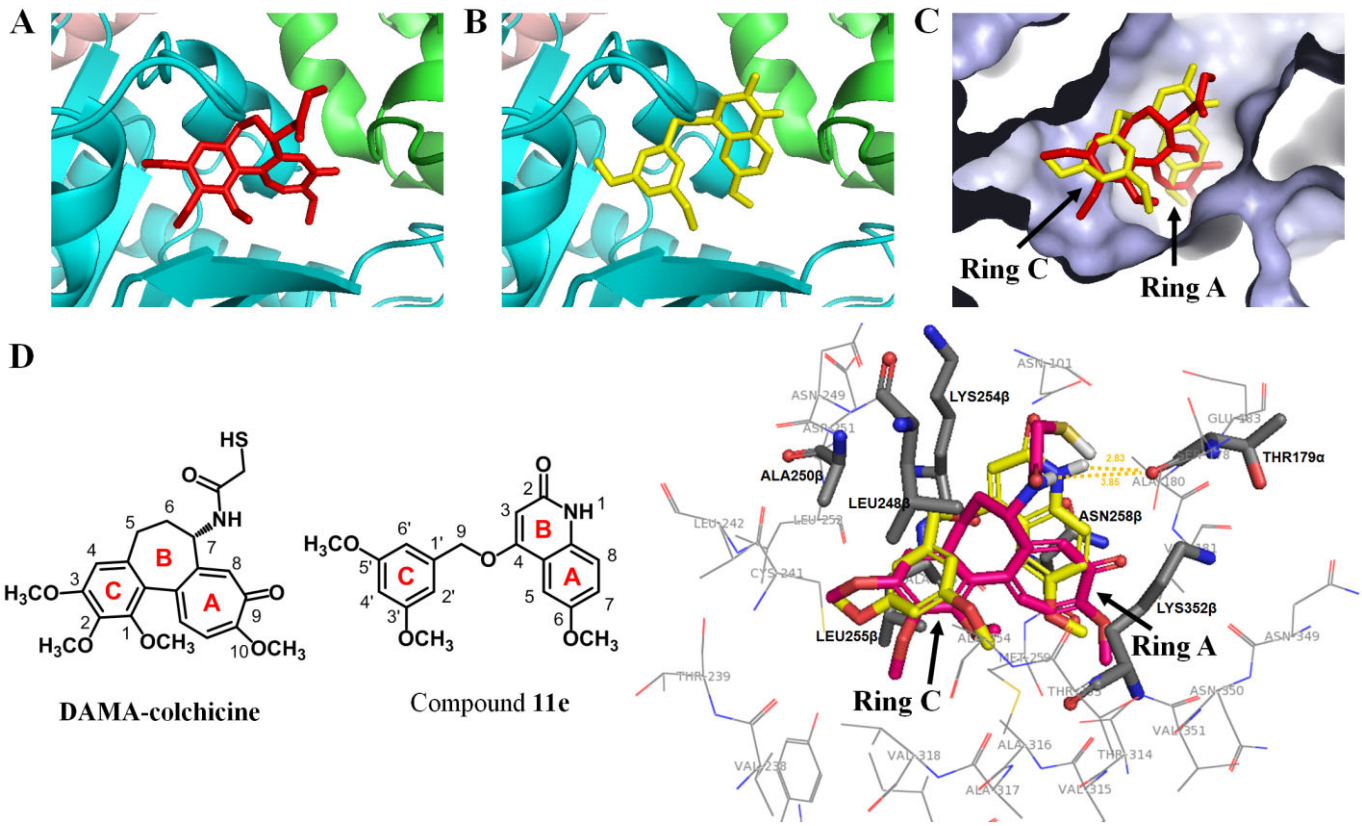

Figure 8

The docked binding mode of **11e** is shown with the binding site of tubulin (PDB entry 1SA0). The figures were performed using PyMol. (A) The binding mode of DAMA-colchicine (red stick model) and tubulin. (B) The binding mode of **11e** (yellow stick model) and tubulin. (C) DAMA-colchicine and **11e** occupy similar binding space in tubulin (shown as surface of tubulin cavity). (D) The superimposition of DAMA-colchicine and **11e**.

exhibited improved cytotoxicity in comparison with 6,7-methylenedioxy-4-(2,4-dimethoxyphenyl)quinolin-2(1*H*)-one, the most potent 4-PQ analog previously reported (IC_{50} 0.4, 1.0, 0.9 and 7.4 μM against the four tumour cell lines) (Chen *et al.*, 2013b). SAR study on these new compounds revealed that a 3′,5′-dimethoxybenzyloxy moiety, linked at the 4-position of a 6-methoxy-2-quinolone backbone is most favourable for increased antiproliferative activity.

In the NCI-60 assay, compounds **9b**, **9c**, **9e** and **11e** showed broad-spectrum antitumour properties at the nanomolar level. In particular, compound **11e** not only inhibited the growth of numerous cancer cell lines at the low micromolar range, but also exhibited high selectivity against COLO 205 (colon cancer). Furthermore, the preliminary biological studies indicated that compound **11e** inhibited cell growth and induced apoptosis in COLO 205 cells. Based on these results, compound **11e** has been identified as a promising hit and candidate for future development.

Investigation of the anticancer activity of this novel 2-quinolone analogue provided data indicating that **11e** exerted highly antiproliferative activity and cytotoxicity against COLO 205 cells in a dose- and time-dependent manner (Figure 6C), resulting in G2/M arrest and apoptosis (Figure 7A). Microtubules are important cellular targets for anticancer therapy because of their key role in mitosis (Perez, 2009). Microtubule-targeting agents, including the taxanes, *Vinca* alkaloids and colchicine, bind to different sites on tubulin and affect stabilization or destabilization of microtubule dynamics (Dumontet and Jordan, 2010). To clarify the molecular regulation of **11e** in G2/M arrest, we first examined its influence on microtubules. Our data showed that **11e** results in the depolymerization of microtubules in COLO 205 cells and disrupts intracellular microtubule networks in intact cells, as shown in the immunofluorescence studies (Figure 7B). Treatment of **11e** for 24 h resulted in microtubule changes similar to those induced by colchicine. The docked conformation of **11e** was selected as a working model (Figure 8), based on its similarity to the crystal structure of the bound conformation of DAMA-colchicine in tubulin. The superimposition of **11e** and DAMA-colchicine based on A ring showed an extensive overlap of the 2-quinolone cores and C rings of both molecules had similar orientations. This result supports the hypothesis that the spatial arrangement of the aromatic A and C ring plays a crucial role in the activity and binding of compounds that bind to the main binding site of the colchicine domain on α- and β-tubulin. These findings characterize **11e** as an antimitotic agent.

Previous investigations have reported that cyclin B1/CDK1 complexes are involved in the regulation of G2/M phase and M phase transitions (Peters, 2006; Yang *et al.*,

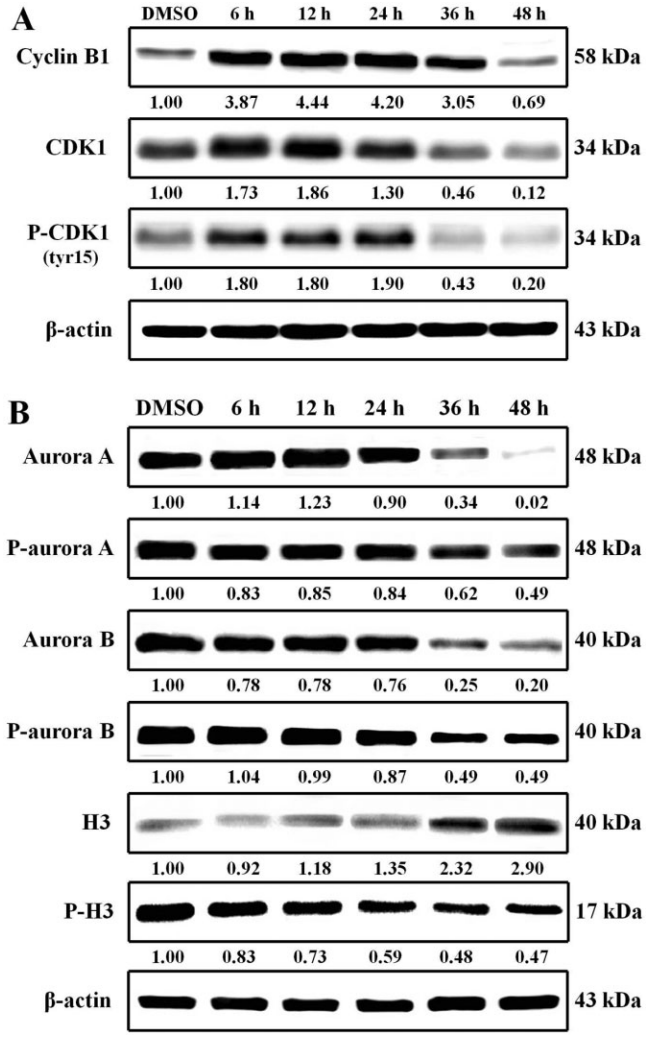

Figure 9

Compound **11e** increased G2/M phase checkpoint protein expression. COLO 205 cells were treated with 50 nM **11e** for the indicated time periods and lysed for protein extraction. Protein samples (40 μg protein per lane) were separated using 10% SDS-PAGE and subjected to immunoblotting with antibodies specific to cyclin B1, CDK1, phospho-CDK1 (A), aurora A, phospho-aurora A, aurora B, phospho-aurora B, H3, phospho-H3 (B) and β-actin ($n = 3$ independent experiments). β-Actin was used as a loading control.

2009). Our data showed increased levels of cyclin B1/CDK1 after **11e** treatment within 6 to 24 h of treatment (Figure 9A). These results reveal that treatment with **11e** not only directly contributes to disrupting microtubules in COLO 205 cells, but also induces accumulation of cyclin B1/CDK1. Aurora kinases also play important roles in chromosome alignment, segregation and cytokinesis during mitosis (Andrews, 2005; Fu *et al.*, 2007; Yang *et al.*, 2007). Our data showed decreased aurora A, phospho-aurora A, aurora B, phospho-aurora B and phospho-H3 expression after **11e** treatment (Figure 9B). Therefore, **11e** inhibited the growth of COLO 205 cells and arrested cells at the G2/M phase through the inactivation of aurora kinases.

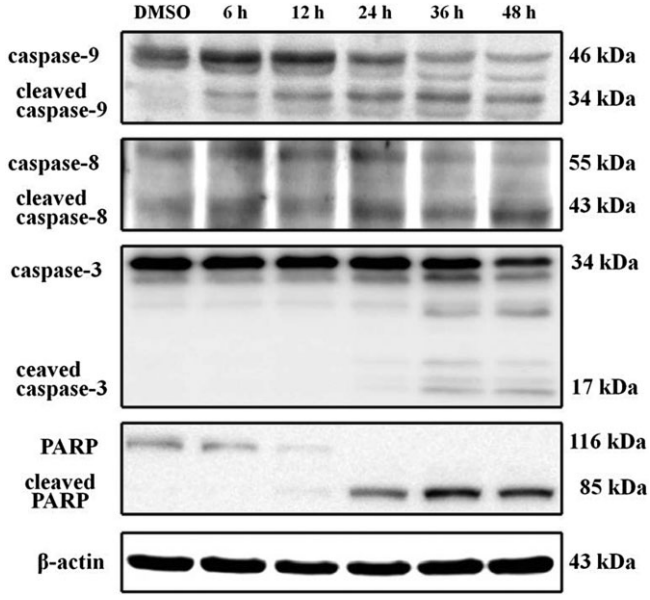

Figure 10

Compound **11e** induced caspase-3, caspase-8 and caspase-9 activity in COLO 205 cells. COLO 205 cells were treated with 50 nM **11e** for the indicated times and lysed for protein extraction. Protein samples (40 μg protein per lane) were separated using 10% SDS-PAGE and subjected to immunoblotting with antibodies specific to caspase-9, caspase-8, caspase-3, PARP and β-actin ($n = 3$ independent experiments). β-Actin was used as a loading control.

Apoptosis induced by antimitotic agents is known to be related to alterations of cellular signalling pathways (Bhalla, 2003; Jordan and Wilson, 2004). Compound **11e** not only demonstrated broad-spectrum anticancer effects but also produced apoptosis, as shown by the findings of annexin V/PI in COLO 205 cells. Apoptosis regulators have been extensively studied and provide the basis for novel therapeutic strategies aimed at promoting tumour cell death (Lowe and Lin, 2000; Ghobrial *et al.*, 2005). To investigate the involvement of apoptosis pathways in **11e**-mediated cytotoxicity, we assessed the caspase cascades. The results showed that **11e** induced significant caspase-3, caspase-8 and caspase-9 activities (Figure 10). Moreover, caspase 8 is one of the caspases involved in the extrinsic pathway, while caspase-9 acts in the intrinsic pathway.

The intrinsic pathway is initiated with loss of membrane potential in mitochondria and then the release of cytochrome *c*, AIF and Endo G from the mitochondria into the cytosol. Cytochrome *c* in conjunction with Apaf-1 and procaspase-9 form an apoptosome. This complex promotes the activation of caspase-9, which in turn activates caspase-3, leading to apoptosis (Green and Reed, 1998; Dlamini *et al.*, 2004; Eberle *et al.*, 2007). Proteolytic degradation of PARP, a substrate of caspase-3, indicated that caspase activation was involved in **11e**-induced apoptosis in COLO 205 cells (Figure 10B). To confirm that mitochondria-mediated intrinsic pathways were involved in **11e**-mediated apoptosis, we further monitored the changes of mitochondrial membrane potential. Our data showed a loss of mitochondrial membrane potential in cells treated with compound **11e**

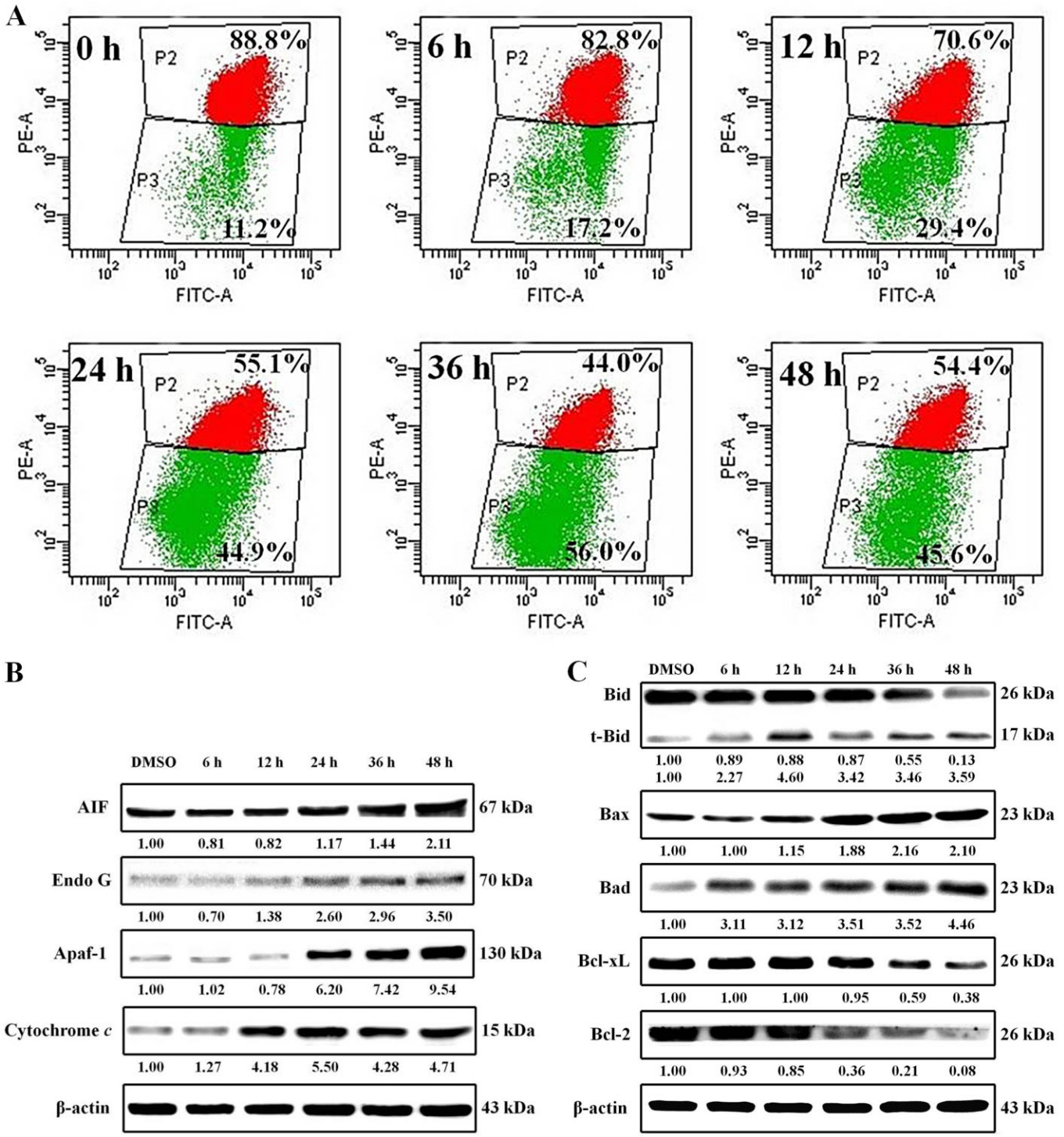

Figure 11

Compound **11e** induced the mitochondrial apoptosis pathway in COLO 205 cells. (A) Effects of **11e** on mitochondrial membrane potential in COLO 205 cells. Cells (1×10^6 cells·mL^{-1}) were untreated or treated with **11e** (50 nM, 6–48 h) to induce apoptosis. Cells were stained with JC-1 and analysed by flow cytometry. (B) COLO 205 cells were treated with 50 nM **11e** for the indicated times and lysed for protein extraction. Protein samples (40 μg protein per lane) were separated using 10% SDS-PAGE and subjected to immunoblotting with antibodies specific to AIF, Endo G, Apaf-1, cytochrome *c* and β-actin ($n = 3$ independent experiments). (C) Compound **11e** affected Bcl-2 family proteins in COLO 205 cells. COLO 205 cells were treated with 50 nM **11e** for the indicated times and lysed for protein extraction. Protein samples (40 μg protein per lane) were separated using 10% SDS-PAGE and subjected to immunoblotting with antibodies specific to Bid, Bax, Bad, Bcl-xL, Bcl-2 and β-actin ($n = 3$ independent experiments). β-Actin was used as a loading control.

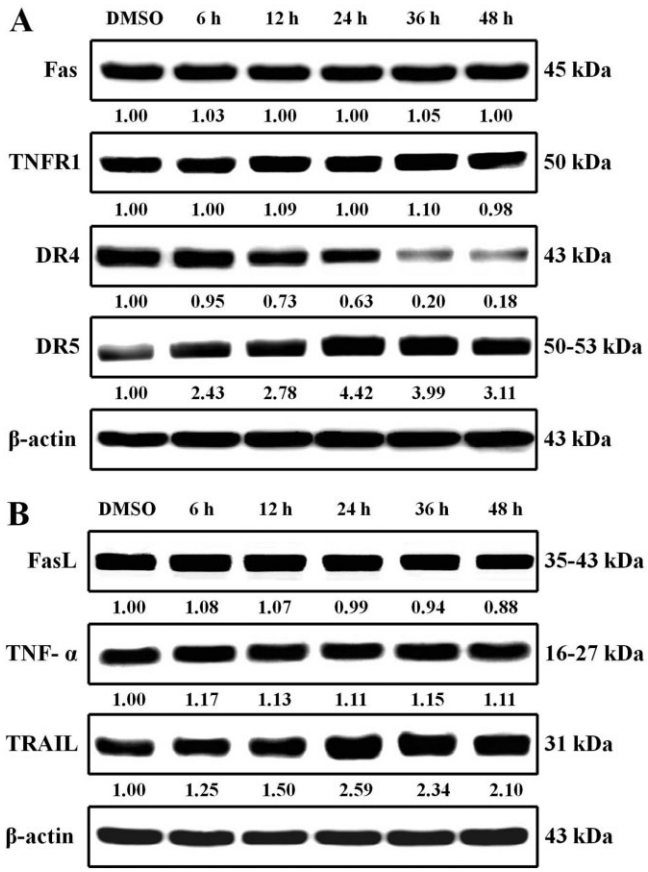

Figure 12

Compound **11e**-induced death receptor apoptosis pathways in COLO 205 cells. COLO 205 cells were treated with 50 nM **11e** for the indicated times and lysed for protein extraction. Protein samples (40 μg protein per lane) were separated using 10% SDS-PAGE and subjected to immunoblotting with antibodies specific to Fas, TNFR1, DR4, DR5 (A), FasL, TNF-α, TRAIL (B) and β-actin (n = 3 independent experiments). β-Actin was used as a loading control.

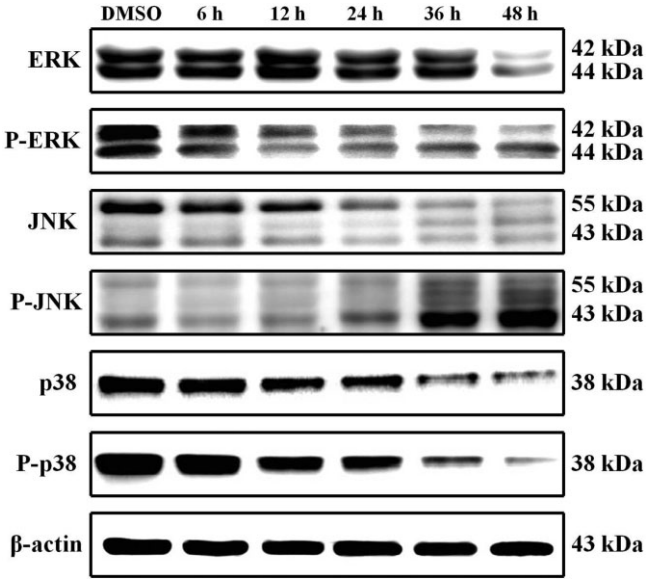

Figure 13

Expression of MAPKs in the **11e**-treated COLO 205 cells. COLO 205 cells were treated with 50 nM **11e** for the indicated times and lysed for protein extraction. Protein samples (40 μg protein per lane) were separated using 10% SDS-PAGE and subjected to immunoblotting with antibodies specific to ERK1/2, phospho-ERK1/2, JNK, phospho-JNK, p38, phospho-p38 and β-actin (n = 3 independent experiments). β-Actin was used as a loading control.

(Figure 11A). Figure 11B shows that compound **11e** induce a time-dependent effect on cytochrome *c*, AIF and Endo G translocation from the mitochondria into the cytosol. The Bcl-2 family proteins largely mediate the mitochondrial apoptotic pathway. These proteins include proapoptotic members, such as Bax and Bad, which promote mitochondrial permeability, and anti-apoptotic members, such as Bcl-2 and Bcl-xL, which inhibit the proapoptotic protein effects or inhibit the mitochondrial release of cytochrome *c* (Antonsson *et al.*, 1997; Bagci *et al.*, 2006). Overexpression of Bcl-2 increases cell survival by suppressing apoptosis. Bax levels increase in conjunction with Bax inhibition of Bcl-2 and the cells undergo apoptosis (Gross *et al.*, 1999; Vela *et al.*, 2013). The present results showed that **11e** treatment resulted in a decrease in the level of anti-apoptotic proteins Bcl-xL and Bcl-2 as well as an increase in the level of proapoptotic protein Bax and Bad (Figure 11C).

The extrinsic pathway is initiated by ligation of transmembrane death receptors (Fas, DR4/5 and TNFR1) with their respective ligands (FasL, TRAIL and TNFα) triggering the formation of a death-inducing complex to active caspase-8, which in turn cleaves and activates caspase-3 (Ashkenazi and Dixit, 1998; Thorburn, 2004). Enhanced TRAIL expression and stimulation of DR4- and/or DR5-induced apoptosis has been shown in certain types of cancers, including colon, ovarian, prostate, bladder and chronic lymphocytic leukaemia (O'Flaherty *et al.*, 2006; Lee *et al.*, 2011; Thomas *et al.*, 2013). In the present study, we found that **11e** treatment up-regulated the expression of the DR5 protein and influenced the expression of TRAIL (Figure 12). Caspase-8 is activated by the death receptor. Activated caspase-8 can cleave and activate downstream caspase-3. On the other hand, caspase-8 can induce Bid cleavage and the cleaved Bid causes cytochrome *c* efflux from mitochondria, then activation of caspase-9 and caspase-3. We showed that **11e** induced the cleavage of full-length Bid producing truncated Bid (t-Bid, 17 kDa), which translocated to the mitochondria. These findings together suggest that **11e** induced apoptosis by activating both intrinsic and extrinsic signalling pathways.

MAPKs, which belong to a large family of serine-threonine kinase, are critical mediators of the cell membrane to nucleus signal transduction in response to various extracellular stimuli (Pearson *et al.*, 2001; Fang and Richardson, 2005). The three major subfamilies of MAPK include the ERKs, JNK and p38. Recent studies have shown that JNKs and p38 pathways are associated with increased apoptosis, whereas the ERK1/2 pathway is shown to suppress apoptosis. In our experiments, we observed that after 24 h incubation, **11e** increased levels of phosphorylated JNK in COLO 205 cells (Figure 13). TRAIL can also activate JNK through the

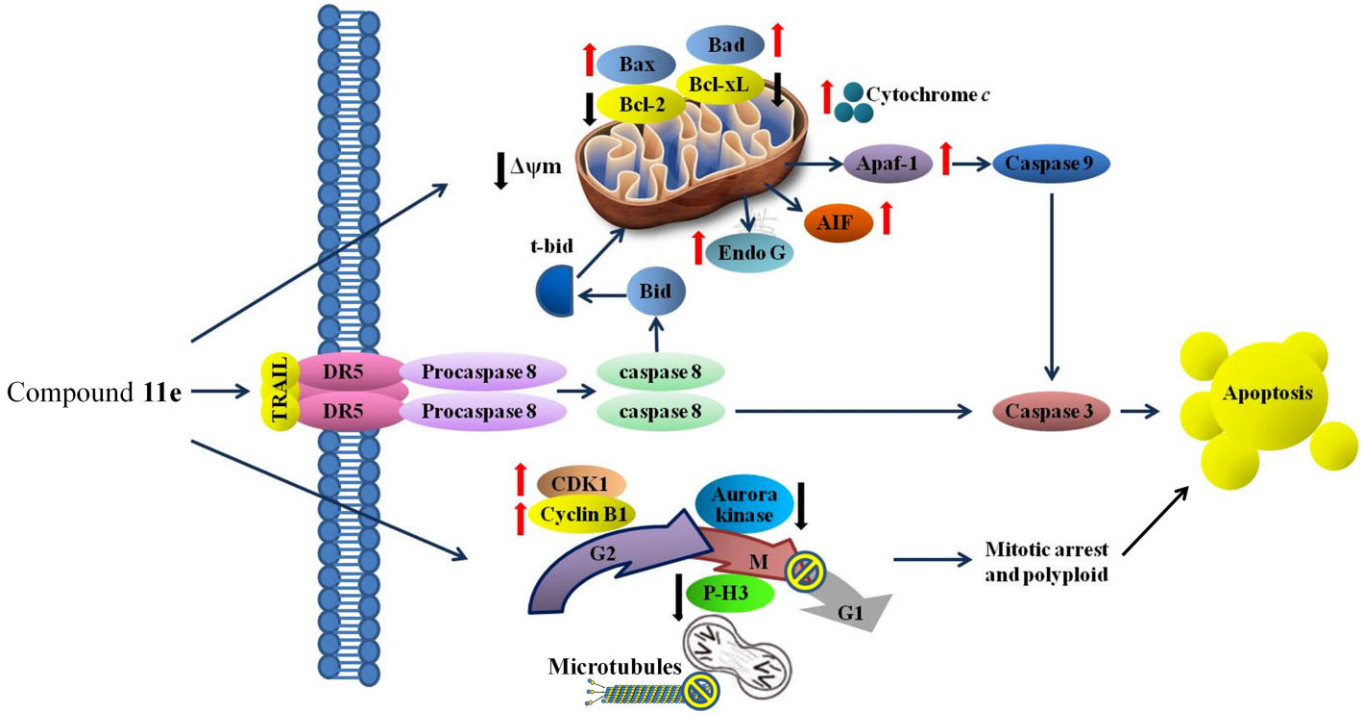

Figure 14
The signalling pathways of **11e**-induced G2/M phase arrest and apoptosis in human colon cancer COLO 205 cells.

adaptor molecules TRAF2 and RIP (Lin *et al.*, 2000) and JNK is activated by TRAIL in colon cancer cells (Mahalingam *et al.*, 2009). In our study, **11e**-activated JNK might play a mediated role in TRAIL-induced apoptosis in COLO 205 cells.

In summary, our present study has identified novel 4-benzyloxyquinolin-2(1*H*)-ones as potent inducers of apoptosis in a range of cancer cells. This new series of compounds could be further exploited to obtain analogues with higher activity for cancer chemotherapy. Figure 14 summarizes the molecular signalling pathways induced by **11e**. We demonstrated that compound **11e** exhibited broad-spectrum anticancer properties against several solid tumour cells and exerted potential anticancer activity against COLO 205 cells. Based on our mechanistic results, compound **11e** caused tubulin depolymerization, aurora A and aurora B inactivation, G2/M phase arrest, polyploidy and subsequent apoptosis via both intrinsic and extrinsic apoptotic pathways. These findings suggest that compound **11e** has potential use as a novel therapeutic agent for the treatment of human colon carcinoma.

Acknowledgements

This investigation was supported by research grants NSC 95-2320-B-039-011-MY3 and NSC 98-2628-B-039-018-MY3 from the National Science Council of the Republic of China awarded to L-J. H. as well as CA177584 from the National Cancer Institute, NIH awarded to K-H. L. The authors thank the US National Cancer Institute (NCI) for screening compounds by the Developmental Therapeutics Program at NCI (Anticancer Screening Program; http://dtp.cancer.gov).

Author contributions

Y-F. C., L-J. H. and K-H. L. conceived and designed the experiments. Y-F. C., Y-C. L., C-F. W., T-C. S., H-Y. L. and M-H. H. performed the experiments. Y-F. C. and Y-C. L. analysed the data. Y-F. C., Y-C. L., S. L. M-N., Y. Z., K-H. L. and L-J. H. wrote the paper. L-C. C. and S-C. K. submitted the compounds to NCI.

Conflict of interest

The authors declare that there are no conflicts of interest.

References

Abonia R, Insuasty D, Castillo J, Insuasty B, Quiroga J, Nogueras M *et al.* (2012). Synthesis of novel quinoline-2-one based chalcones of potential anti-tumor activity. Eur J Med Chem 57: 29–40.

Ahmed N, Brahmbhatt KG, Sabde S, Mitra D, Singh IP, Bhutani KK (2010). Synthesis and anti-HIV activity of alkylated quinoline 2,4-diols. Bioorg Med Chem 18: 2872–2879.

Ahmed N, Brahmbhatt KG, Singh IP, Bhutani KK (2011). Efficient chemoselective alkylation of quinoline 2,4-diol derivatives in water. J Heterocycl Chem 48: 237–240.

Ahvale AB, Prokopcová H, Šefčovičová J, Steinschifter W, Täubl AE, Uray G *et al*. (2008). 4-Cyano-6,7-dimethoxycarbostyrils with solvent- and pH-independent high fluorescence quantum yields and emission maxima. Eur J Org Chem 2008: 563–571.

Alexander SPH, Benson HE, Faccenda E, Pawson AJ, Sharman JL Spedding M *et al* (2013a). The Concise Guide to PHARMACOLOGY 2013/14: Enzymes. Br J Pharmacol 170: 1797–1867.

Alexander SPH, Benson HE, Faccenda E, Pawson AJ, Sharman JL Spedding M *et al* (2013b). The Concise Guide to PHARMACOLOGY 2013/14: Catalytic Receptors. Br J Pharmacol 170: 1676–1705.

Al-Obaid AM, Abdel-Hamide SG, El-Kashef HA, Abdel-Aziz AAM, El-Azab AS, Al-Khamees HA *et al*. (2009). Substituted quinazolines, part 3. Synthesis, *in vitro* antitumor activity and molecular modeling study of certain 2-thieno-4(3H)-quinazolinone analogs. Eur J Med Chem 44: 2379–2391.

Andrews PD (2005). Aurora kinases: shining lights on the therapeutic horizon? Oncogene 24: 5005–5015.

Antonsson B, Conti F, Ciavatta A, Montessuit S, Lewis S, Martinou I *et al*. (1997). Inhibition of Bax channel-forming activity by Bcl-2. Science 277: 370–372.

Arya K, Agarwal M (2007). Microwave prompted multigram synthesis, structural determination, and photo-antiproliferative activity of fluorinated 4-hydroxyquinolinones. Bioorg Med Chem Lett 17: 86–93.

Ashkenazi A, Dixit VM (1998). Death receptors: signaling and modulation. Science 281: 1305–1308.

Baba A, Kawamura N, Makino H, Ohta Y, Taketomi S, Sohda T (1996). Studies on disease-modifying antirheumatic drugs: synthesis of novel quinoline and quinazoline derivatives and their anti-inflammatory effect. J Med Chem 39: 5176–5182.

Bagci EZ, Vodovotz Y, Billiar TR, Ermentrout GB, Bahar I (2006). Bistability in apoptosis: roles of bax, bcl-2, and mitochondrial permeability transition pores. Biophys J 90: 1546–1559.

Bhalla KN (2003). Microtubule-targeted anticancer agents and apoptosis. Oncogene 22: 9075–9086.

Boyd MR, Paull KD (1995). Some practical considerations and applications of the national cancer institute in vitro anticancer drug discovery screen. Drug Dev Res 34: 91–109.

Brunelle JK, Letai A (2009). Control of mitochondrial apoptosis by the Bcl-2 family. J Cell Sci 122: 437–441.

Buckle DR, Cantello BCC, Smith H, Spicer BA (1975). 4-Hydroxy-3-nitro-2-quinolones and related compounds as inhibitors of allergic reactions. J Med Chem 18: 726–732.

Cai SX, Zhou Z-L, Huang J-C, Whittemore ER, Egbuwoku ZO, Lü Y *et al*. (1996). Synthesis and structure–activity relationships of 1,2,3,4-tetrahydroquinoline-2,3,4-trione 3-oximes: novel and highly potent antagonists for NMDA receptor glycine site. J Med Chem 39: 3248–3255.

Chae M-Y, Swenn K, Kanugula S, Dolan ME, Pegg AE, Moschel RC (1995). 8-Substituted O6-benzylguanine, substituted 6(4)-(Benzyloxy)pyrimidine, and related derivatives as inactivators of human O6-alkylguanine-DNA alkyltransferase. J Med Chem 38: 359–365.

Chan SH, Chui CH, Chan SW, Kok SHL, Chan D, Tsoi MYT *et al*. (2012). Synthesis of 8-hydroxyquinoline derivatives as novel antitumor agents. ACS Med Chem Lett 4: 170–174.

Chen T-C, Yu D-S, Huang K-F, Fu Y-C, Lee C-C, Chen C-L *et al*. (2013a). Structure-based design, synthesis and biological evaluation of novel anthra[1,2-d]imidazole-6,11-dione homologues as potential antitumor agents. Eur J Med Chem 69: 278–293.

Chen Y-F, Lin Y-C, Huang P-K, Chan H-C, Kuo S-C, Lee K-H *et al*. (2013b). Design and synthesis of 6,7-methylenedioxy-4-substituted phenylquinolin-2(1H)-one derivatives as novel anticancer agents that induce apoptosis with cell cycle arrest at G2/M phase. Bioorg Med Chem 21: 5064–5075.

Cheng G, Hao H, Dai M, Liu Z, Yuan Z (2013). Antibacterial action of quinolones: from target to network. Eur J Med Chem 66: 555–562.

Chung HS, Woo WS (2001). A quinolone alkaloid with antioxidant activity from the aleurone layer of anthocyanin-pigmented rice. J Nat Prod 64: 1579–1580.

Coombs TC, Tanega C, Shen M, Wang JL, Auld DS, Gerritz SW *et al*. (2013). Small-molecule pyrimidine inhibitors of the cdc2-like (Clk) and dual specificity tyrosine phosphorylation-regulated (Dyrk) kinases: development of chemical probe ML315. Bioorg Med Chem Lett 23: 3654–3661.

Cornut D, Lemoine H, Kanishchev O, Okada E, Albrieux F, Beavogui AH *et al*. (2013). Incorporation of a 3-(2,2,2-trifluoroethyl)-gamma-hydroxy-gamma-lactam motif in the side chain of 4-aminoquinolines. Syntheses and antimalarial activities. J Med Chem 56: 73–83.

Daniels DS, Mol CD, Arvai AS, Kanugula S, Pegg AE, Tainer JA (2000). Active and alkylated human AGT structures: a novel zinc site, inhibitor and extrahelical base binding. EMBO J 19: 1719–1730.

Deng X-Q, Wei C-X, Song M-X, Chai K-Y, Sun Z-G, Quan Z-S (2010). Synthesis and studies on anticonvulsant and antidepressant activities of 5-alkoxy-tetrazolo[1,5-a]quinolines. Bull Korean Chem Soc 31: 447–452.

Dlamini Z, Mbita Z, Zungu M (2004). Genealogy, expression, and molecular mechanisms in apoptosis. Pharmacol Ther 101: 1–15.

Dolan ME, Pegg AE (1997). O6-benzylguanine and its role in chemotherapy. Clin Cancer Res 3: 837–847.

Doležal K, Popa I, Kryštof V, Spíchal L, Fojtíková M, Holub J *et al*. (2006). Preparation and biological activity of 6-benzylaminopurine derivatives in plants and human cancer cells. Bioorg Med Chem 14: 875–884.

Dumontet C, Jordan MA (2010). Microtubule-binding agents: a dynamic field of cancer therapeutics. Nat Rev Drug Discov 9: 790–803.

Eberle J, Fecker LF, Forschner T, Ulrich C, Rowert-Huber J, Stockfleth E (2007). Apoptosis pathways as promising targets for skin cancer therapy. Br J Dermatol 156 (Suppl. 3): 18–24.

Elmore S (2007). Apoptosis: a review of programmed cell death. Toxicol Pathol 35: 495–516.

van Engeland M, Nieland LJ, Ramaekers FC, Schutte B, Reutelingsperger CP (1998). Annexin V-affinity assay: a review on an apoptosis detection system based on phosphatidylserine exposure. Cytometry 31: 1–9.

Fang JY, Richardson BC (2005). The MAPK signalling pathways and colorectal cancer. Lancet Oncol 6: 322–327.

Fesik SW (2005). Promoting apoptosis as a strategy for cancer drug discovery. Nat Rev Cancer 5: 876–885.

Fiorito J, Saeed F, Zhang H, Staniszewski A, Feng Y, Francis YI *et al*. (2013). Synthesis of quinoline derivatives: discovery of a potent

and selective phosphodiesterase 5 inhibitor for the treatment of Alzheimer's disease. Eur J Med Chem 60: 285–294.

Fischer U, Schulze-Osthoff K (2005). Apoptosis-based therapies and drug targets. Cell Death Differ 12: 942–961.

Folger O, Jerby L, Frezza C, Gottlieb E, Ruppin E, Shlomi T (2011). Predicting selective drug targets in cancer through metabolic networks. Mol Syst Biol 7: 501.

Font M, González Á, Palop JA, Sanmartín C (2011). New insights into the structural requirements for pro-apoptotic agents based on 2,4-diaminoquinazoline, 2,4-diaminopyrido[2,3-d]pyrimidine and 2,4-diaminopyrimidine derivatives. Eur J Med Chem 46: 3887–3899.

Freeman GA, Andrews Iii CW 3rd, Hopkins AL, Lowell GS, Schaller LT, Cowan JR *et al*. (2004). Design of non-nucleoside inhibitors of HIV-1 reverse transcriptase with improved drug resistance properties. 2. J Med Chem 47: 5923–5936.

Fu J, Bian M, Jiang Q, Zhang C (2007). Roles of aurora kinases in mitosis and tumorigenesis. Mol Cancer Res 5: 1–10.

Ghobrial IM, Witzig TE, Adjei AA (2005). Targeting apoptosis pathways in cancer therapy. CA Cancer J Clin 55: 178–194.

Gibson AE, Arris CE, Bentley J, Boyle FT, Curtin NJ, Davies TG *et al*. (2002). Probing the ATP ribose-binding domain of cyclin-dependent kinases 1 and 2 with O(6)-substituted guanine derivatives. J Med Chem 45: 3381–3393.

Green DR, Reed JC (1998). Mitochondria and apoptosis. Science 281: 1309–1312.

Gross A, McDonnell JM, Korsmeyer SJ (1999). BCL-2 family members and the mitochondria in apoptosis. Genes Dev 13: 1899–1911.

Guo L-J, Wei C-X, Jia J-H, Zhao L-M, Quan Z-S (2009). Design and synthesis of 5-alkoxy-[1,2,4]triazolo[4,3-a]quinoline derivatives with anticonvulsant activity. Eur J Med Chem 44: 954–958.

He J, Lion U, Sattler I, Gollmick FA, Grabley S, Cai J *et al*. (2005). Diastereomeric quinolinone alkaloids from the marine-derived fungus *Penicillium janczewskii*. J Nat Prod 68: 1397–1399.

Holbeck SL (2004). Update on NCI in vitro drug screen utilities. Eur J Cancer 40: 785–793.

Holbeck SL, Collins JM, Doroshow JH (2010). Analysis of food and drug administration-approved anticancer agents in the NCI60 panel of human tumor cell lines. Mol Cancer Ther 9: 1451–1460.

Hopkins AL, Ren J, Milton J, Hazen RJ, Chan JH, Stuart DI *et al*. (2004). Design of non-nucleoside inhibitors of HIV-1 reverse transcriptase with improved drug resistance properties. 1. J Med Chem 47: 5912–5922.

Ito C, Itoigawa M, Furukawa A, Hirano T, Murata T, Kaneda N *et al*. (2004). Quinolone alkaloids with nitric oxide production inhibitory activity from *Orixa japonica*. J Nat Prod 67: 1800–1803.

Jorda R, Havlicek L, McNae IW, Walkinshaw MD, Voller J, Sturc A *et al*. (2011). Pyrazolo[4,3-d]pyrimidine bioisostere of roscovitine: evaluation of a novel selective inhibitor of cyclin-dependent kinases with antiproliferative activity. J Med Chem 54: 2980–2993.

Jordan MA, Wilson L (2004). Microtubules as a target for anticancer drugs. Nat Rev Cancer 4: 253–265.

Kappe T, Karem AS, Stadlbauer W (1988). Synthesis of benzo-halogenated 4-hydroxy-2(1H)-quinolones. J Heterocycl Chem 25: 857–862.

Kaufmann SH, Earnshaw WC (2000). Induction of apoptosis by cancer chemotherapy. Exp Cell Res 256: 42–49.

Keen N, Taylor S (2004). Aurora-kinase inhibitors as anticancer agents. Nat Rev Cancer 4: 927–936.

LaPlante SR, Bilodeau F, Aubry N, Gillard JR, O'Meara J, Coulombe R (2013). N- versus O-alkylation: utilizing NMR methods to establish reliable primary structure determinations for drug discovery. Bioorg Med Chem Lett 23: 4663–4668.

Lee J-C, Chou L-C, Huang C-H, Chung J-G, Huang L-J, Lee K-H *et al*. (2011). CHM-1 induces apoptosis via p38-mediated upregulation of DR5 expression in human ovarian cancer SKOV3 cells. Eur J Pharmacol 670: 96–104.

Lewis FD, Reddy GD, Elbert JE, Tillberg BE, Meltzer JA, Kojima M (1991). Lewis acid catalysis of photochemical reactions. 10. Spectroscopy and photochemistry of 2-quinolones and their Lewis acid complexes. J Org Chem 56: 5311–5318.

Lilienkampf A, Mao J, Wan B, Wang Y, Franzblau SG, Kozikowski AP (2009). Structure-activity relationships for a series of quinoline-based compounds active against replicating and nonreplicating *Mycobacterium tuberculosis*. J Med Chem 52: 2109–2118.

Lin Y, Devin A, Cook A, Keane MM, Kelliher M, Lipkowitz S *et al*. (2000). The death domain kinase RIP is essential for TRAIL (Apo2L)-induced activation of IκB kinase and c-Jun N-terminal kinase. Mol Cell Biol 20: 6638–6645.

Liu J, Grimison B, Maller JL (2007). New insight into metaphase arrest by cytostatic factor: from establishment to release. Oncogene 26: 1286–1289.

Longley DB, Harkin DP, Johnston PG (2003). 5-Fluorouracil: mechanisms of action and clinical strategies. Nat Rev Cancer 3: 330–338.

Lowe SW, Lin AW (2000). Apoptosis in cancer. Carcinogenesis 21: 485–495.

Mahalingam D, Keane M, Pirianov G, Mehmet H, Samali A, Szegezdi E (2009). Differential activation of JNK1 isoforms by TRAIL receptors modulate apoptosis of colon cancer cell lines. Br J Cancer 100: 1415–1424.

Mohamed EHA (1991). One-step synthesis of 4-hydroxycarbostyrils .6. J Chem Soc Pak 13: 166–168.

Moradi-e-Rufchahi EOL (2010). Synthesis of 6-chloro and 6-fluoro-4-hydroxyl-2-quinolone and their azo disperse dyes. Chin Chem Lett 21: 542–546.

Mosmann T (1983). Rapid colorimetric assay for cellular growth and survival: application to proliferation and cytotoxicity assays. J Immunol Methods 65: 55–63.

Mott BT, Tanega C, Shen M, Maloney DJ, Shinn P, Leister W *et al*. (2009). Evaluation of substituted 6-arylquinazolin-4-amines as potent and selective inhibitors of cdc2-like kinases (Clk). Bioorg Med Chem Lett 19: 6700–6705.

Mukherjee S, Pal M (2013). Quinolines: a new hope against inflammation. Drug Discov Today 18: 389–398.

Nadaraj V, Selvi ST, Sasi R (2006). Microwave-assisted synthesis of quinoline alkaloids: 4-methoxy-1-methyl-2-quinolinone and its analogs. ARKIVOC 10: 82–89.

Nakashima K-I, Oyama M, Ito T, Akao Y, Witono JR, Darnaedi D *et al*. (2012). Novel quinolinone alkaloids bearing a lignoid moiety and related constituents in the leaves of *Melicope denhamii*. Tetrahedron 68: 2421–2428.

Noolvi MN, Patel HM, Kamboj S, Kaur A, Mann V (2012). 2,6-Disubstituted imidazo[2,1-b][1,3,4]thiadiazoles: search for anticancer agents. Eur J Med Chem 56: 56–69.

O'Flaherty J, Mei Y, Freer M, Weyman CM (2006). Signaling through the TRAIL receptor DR5/FADD pathway plays a role in the apoptosis associated with skeletal myoblast differentiation. Apoptosis 11: 2103–2113.

Oh S, Park SB (2011). A design strategy for drug-like polyheterocycles with privileged substructures for discovery of specific small-molecule modulators. Chem Commun 47: 12754–12761.

Pandey S, Agarwal P, Srivastava K, RajaKumar S, Puri SK, Verma P *et al*. (2013). Synthesis and bioevaluation of novel 4-aminoquinoline-tetrazole derivatives as potent antimalarial agents. Eur J Med Chem 66: 69–81.

Park KK, Lee JJ (2004). Facile synthesis of 4-phenylquinolin-2(1H)-one derivatives from N-acyl-o-aminobenzophenones. Tetrahedron 60: 2993–2999.

Park S-J, Lee J-C, Lee K-I (2007). A facile synthesis of 4-hydroxycoumarin and 4-hydroxy-2-quinolone derivatives. Bull Korean Chem Soc 28: 1203–1205.

Paruch K, Dwyer MP, Alvarez C, Brown C, Chan T-Y, Doll RJ *et al*. (2007). Pyrazolo[1,5-a]pyrimidines as orally available inhibitors of cyclin-dependent kinase 2. Bioorg Med Chem Lett 17: 6220–6223.

Pawson AJ, Sharman JL, Benson HE, Faccenda E, Alexander SP, Buneman OP *et al*.; NC-IUPHAR (2014). The IUPHAR/BPS Guide to PHARMACOLOGY: an expert-driven knowledge base of drug targets and their ligands. Nucl Acids Res 42 (Database Issue): D1098–D1106.

Pearson G, Robinson F, Beers Gibson T, Xu BE, Karandikar M, Berman K *et al*. (2001). Mitogen-activated protein (MAP) kinase pathways: regulation and physiological functions. Endocr Rev 22: 153–183.

Perez EA (2009). Microtubule inhibitors: differentiating tubulin-inhibiting agents based on mechanisms of action, clinical activity, and resistance. Mol Cancer Ther 8: 2086–2095.

Peters J-M (2006). The anaphase promoting complex/cyclosome: a machine designed to destroy. Nat Rev Mol Cell Biol 7: 644–656.

Pirrung MC, Blume F (1999). Rhodium-mediated dipolar cycloaddition of diazoquinolinediones. J Org Chem 64: 3642–3649.

Priya N, Gupta A, Chand K, Singh P, Kathuria A, Raj HG *et al*. (2010). Characterization of 4-methyl-2-oxo-1,2-dihydroquinolin-6-yl acetate as an effective antiplatelet agent. Bioorg Med Chem 18: 4085–4094.

Rastogi T, Hildesheim A, Sinha R (2004). Opportunities for cancer epidemiology in developing countries. Nat Rev Cancer 4: 909–917.

Ravelli RBG, Gigant B, Curmi PA, Jourdain I, Lachkar S, Sobel A *et al*. (2004). Insight into tubulin regulation from a complex with colchicine and a stathmin-like domain. Nature 428: 198–202.

Roy MJ, Vom A, Czabotar PE, Lessene G (2014). Cell death and the mitochondria: therapeutic targeting of the BCL-2 family-driven pathway. Br J Pharmacol 171: 1973–1987.

Ruiz FM, Gil-Redondo R, Morreale A, Ortiz AR, Fábrega C, Bravo J (2008). Structure-based discovery of novel non-nucleosidic DNA alkyltransferase inhibitors: virtual screening and in vitro and in vivo activities. J Chem Inf Model 48: 844–854.

Shoemaker RH (2006). The NCI60 human tumour cell line anticancer drug screen. Nat Rev Cancer 6: 813–823.

Solomon VR, Lee H (2011). Quinoline as a privileged scaffold in cancer drug discovery. Curr Med Chem 18: 1488–1508.

Terashima I, Kohda K (1998). Inhibition of human O6-alkylguanine-DNA alkyltransferase and potentiation of the cytotoxicity of chloroethylnitrosourea by 4(6)-(Benzyloxy)-2,6(4)-diamino-5-(nitro or nitroso)pyrimidine derivatives and analogues. J Med Chem 41: 503–508.

Thomas S, Vasudevan S, Thamkachy R, Lekshmi S, Santhoshkumar T, Rajasekharan K *et al*. (2013). Upregulation of DR5 receptor by the diaminothiazole DAT1 [4-amino-5-benzoyl-2-(4-methoxy phenyl amino) thiazole] triggers an independent extrinsic pathway of apoptosis in colon cancer cells with compromised pro and antiapoptotic proteins. Apoptosis 18: 713–726.

Thorburn A (2004). Death receptor-induced cell killing. Cell Signal 16: 139–144.

Trott O, Olson AJ (2010). AutoDock Vina: improving the speed and accuracy of docking with a new scoring function, efficient optimization, and multithreading. J Comput Chem 31: 455–461.

Vela L, Gonzalo O, Naval J, Marzo I (2013). Direct interaction of bax and bak proteins with bcl-2 homology domain 3 (BH3)-only proteins in living cells revealed by fluorescence complementation. J Biol Chem 288: 4935–4946.

Wang Y, Ai J, Chen Y, Wang L, Liu G, Geng M *et al*. (2011). Synthesis and c-Met kinase inhibition of 3,5-disubstituted and 3,5,7-trisubstituted quinolines: identification of 3-(4-acetylpiperazin-1-yl)-5-(3-nitrobenzylamino)-7-(trifluoromethyl)quinoline as a novel anticancer agent. J Med Chem 54: 2127–2142.

Yang J, Ikezoe T, Nishioka C, Tasaka T, Taniguchi A, Kuwayama Y *et al*. (2007). AZD1152, a novel and selective aurora B kinase inhibitor, induces growth arrest, apoptosis, and sensitization for tubulin depolymerizing agent or topoisomerase II inhibitor in human acute leukemia cells *in vitro* and *in vivo*. Blood 110: 2034–2040.

Yang J-S, Chen G-W, Hsia T-C, Ho H-C, Ho C-C, Lin M-W *et al*. (2009). Diallyl disulfide induces apoptosis in human colon cancer cell line (COLO 205) through the induction of reactive oxygen species, endoplasmic reticulum stress, caspases casade and mitochondrial-dependent pathways. Food Chem Toxicol 47: 171–179.

Zatloukal M, Jorda R, Gucký T, Řezníčková E, Voller J, Pospíšil T *et al*. (2013). Synthesis and in vitro biological evaluation of 2,6,9-trisubstituted purines targeting multiple cyclin-dependent kinases. Eur J Med Chem 61: 61–72.

Zhai D, Jin C, Huang Z, Satterthwait AC, Reed JC (2008). Differential regulation of bax and bak by anti-apoptotic Bcl-2 family proteins Bcl-B and Mcl-1. J Biol Chem 283: 9580–9586.

Zhang S-L, Huang Z-S, Li Y-M, Chan ASC, Gu L-Q (2008). Synthesis of zwitterionic 4-hydroxy-2(1H)-quinolinone derivatives. Tetrahedron 64: 4403–4407.

Zhang Y, Fang Y, Liang H, Wang H, Hu K, Liu X *et al*. (2013). Synthesis and antioxidant activities of 2-oxo-quinoline-3-carbaldehyde Schiff-base derivatives. Bioorg Med Chem Lett 23: 107–111.

Zhu R, Baumann RP, Penketh PG, Shyam K, Sartorelli AC (2013). Hypoxia-selective O6-alkylguanine-DNA alkyltransferase inhibitors: design, synthesis, and evaluation of 6-(benzyloxy)-2-(aryldiazenyl)-9H-purines as prodrugs of O6-benzylguanine. J Med Chem 56: 1355–1359.

Zhuang S-H, Lin Y-C, Chou L-C, Hsu M-H, Lin H-Y, Huang C-H *et al*. (2013). Synthesis and anticancer activity of 2,4-disubstituted furo[3,2-b]indole derivatives. Eur J Med Chem 66: 466–479.

Supporting information

Additional Supporting Information may be found in the online version of this article at the publisher's web-site:

http://dx.doi.org/10.1111/bph.12992

Supporting information includes physical and spectroscopic information, NMR, mass and IR spectra of synthetic target compounds, as well as detailed NCI-60 results for compounds **9b**, **9c**, **9e** and **11e**.

Table S1 NMR spectroscopic data for compound **11e** in DMSO-d_6.

Figure S1 One Dose Mean Graph Program (10 μM) of compound **9b**.

Figure S2 Five doses response curves of compound **9b**.

Figure S3 *In vitro* GI_{50}, TGI and LC_{50} of compound **9b**.

Figure S4 Finger print of *in vitro* GI_{50}, TGI and LC_{50} of compound **9b**.

Figure S5 One Dose Mean Graph Program (10 μM) of compound **9c**.

Figure S6 Five doses response curves of compound **9c**.

Figure S7 *In vitro* GI_{50}, TGI and LC_{50} of compound **9c**.

Figure S8 Finger print of *in vitro* GI_{50}, TGI and LC_{50} of compound **9c**.

Figure S9 One Dose Mean Graph Program (10 μM) of compound **9e**.

Figure S10 Five doses response curves of compound **9e**.

Figure S11 *In vitro* GI_{50}, TGI and LC_{50} of compound **9e**.

Figure S12 Finger print of *in vitro* GI_{50}, TGI and LC_{50} of compound **9e**.

Figure S13 One Dose Mean Graph Program (10 μM) of compound **11e**.

Figure S14 Five doses response curves of compound **11e**.

Figure S15 *In vitro* GI_{50}, TGI and LC_{50} of compound **11e**.

Figure S16 Finger print of *in vitro* GI_{50}, TGI and LC_{50} of compound 11e.

Appendix S1 Spectral copies of $_1$HNMR and $_{13}$C NMR of the synthetic compounds (**5a–i** and **7a–e** ~ **15a–e**).

Appendix S2 Spectral copies of Mass and IR of the synthetic compounds (**5a–i** and **7a–e** ~ **15a–e**).

Appendix S3 The two-dimensional NMR spectra of compound **11e** and NCI-60 results of compounds (**9b**, **9c**, **9e** and **11e**).

Appendix S4 Physical and spectroscopic assignments of the synthetic compounds (**5a–i** and **7a–e** ~ **15a–e**).